Advances in Nano Research, *Vol. 18, No. 2 (2025) 97-116*
https://doi.org/10.12989/anr.2025.18.2.097

Use of metamaterials in graphene origami configuration for an electromagnetoelastic sandwich composite beam

Ruoxin Lin[1], Linyuan Fan*[1], Lixi Liu[2], Mostafa Habibi[3,4,5] and Ibrahim Albaijan[6]

[1]*School of Computer and Big Data, Minjiang University, Fuzhou 350108, Fujian, China*
[2]*Fujian Lead Automatic Equipment Co ltd, Fuzhou 350199, Fujian, China*
[3]*Universidad UTE, Facultad de Arquitectura y Urbanismo, Calle Rumipamba S/N y Bourgeois, Quito, 170147, Ecuador*
[4]*Department of Biomaterials, Saveetha Dental College and Hospital, Saveetha Institute of Medical and Technical Sciences, Chennai, 600 077, India*
[5]*Institute of Research and Development, Duy Tan University, Da Nang, 550000, Viet Nam*
[6]*Mechanical Engineering Department, College of Engineering at Al Kharj, Prince Sattam Bin Abdulaziz University, Al Kharj 16273, Saudi Arabia*

(*Received November 3, 2024, Revised January 23, 2025, Accepted January 28, 2025*)

Abstract. A parametric study on the impact of graphene origami content on the deformation and strain results of a double curved shell is presented. The formulation is extended using the shear deformability property of the kinematic model and the constitutive relations are extended using the overall material properties for the nanofolded composite structures in the thermal environment. The analytical-based method is developed using the energy-based framework for derivation of the governing equations of a nanocomposite double curved shell. The analytical results are extracted using the trigonometric functions in order to satisfy the required boundary conditions.

Keywords: deformation and strain analysis; double curved; nanocomposites; nanofolded structures; novel foldable model; 3D metamaterial nanofillers

1. Introduction

Structural analysis of the advanced materials, structures and systems such as bending, vibration, and stability is necessary for optimized design and is accounted as an important step in the design process. The deformation and strain analysis is used for checking the deformation criteria in advanced design of the structures and machine elements. Analysis of deformation and strain for advanced composite and nanocomposite structures and materials are presented using the analytical, numerical and experimental analysis. The analysis is performed to investigate the impact of important parameters of nanocomposite materials and structures. The main issue in analysis of the nanocomposite structures is estimation of the overall material properties using the experimental, and statistical methods in the literature. In this paper a deformation and strain analysis on the double curved shells composed of graphene origami nanofillers is presented. A literature review on the analysis of the structures using the shear deformation theory, analysis of nanocomposite structures and materials and various nanocomposite structures is presented in this section.

In order to capture impact of the micro size in micro systems and structures, the modified couple stress-based formulation was employed for nonlinear static/dynamic analysis of the nanocomposite porous layers by Tao and Dai (2022). The time-varying solution was provide using Newmark integration method. The isogeometric analysis was provided for investigating the numerical analysis. There are some novel hybrid analysis for investigating the effect of graphene origami characteristics on the static analysis of composite sandwich plate sandwiched between two piezomagnetic layers. A higher-order modeling of the cylindrical panel was developed for dynamic results of a graphene origami reinforced cylindrical panel by Vali and Arefi (2023). To investigate higher order deformation, stress and strain variation in a cylindrical shell, a higher order kinematic modeling was employed. In order to present a more accurate analysis, Wang *et al*. (2024a) developed a stretchable model for dynamic analysis of graphene origami reinforced sport plate. Impact of initial electric potential was studied on the bending responses of graphene nanoplatelets reinforced cylindrical sandwich shell by Zhang *et al*. (2024c). Jin *et al*. (2024) studied interaction of foldability and thermal loads on the bending results of a higher order shell reinforced with graphene origami. Ma *et al*. (2023) studied the impact of micro scale parameters on the static and dynamic results of a microplate using the strain gradient theory. There are some novel works on the application of nanocomposite materials in the chemical engineering by (Bai *et al*. 2023, 2024a, b, c, 2025).

Yu *et al*. (2024a) presented a study for investigating the simultaneous impact of multi field loading and graphene origami characteristics on the responses of sandwich composite reinforced curved beam. Huang *et al*. (2024) developed a new mathematical solution for investigating the

*Corresponding author, Ph.D.,
E-mail: fanlinyuan@mju.edu.cn

ISSN: 2287-237X (Print), 2287-2388 (Online)

impact of various boundary conditions on the bending responses of golf club cylindrical shell. Some important works on the impact of graphene origami in advanced structures and systems can be observed in the literature. Arefi *et al*. (2019) illustrated a large parametric analysis for investigating the impact of various characteristics of graphene nanoplatelets on the bending analysis of composite curved nanobeam using a shear deformable model. An investigation on the convergence of the results with changes of layer's number was presented. Furthermore, the size dependent analysis was carefully discusses using the nonlocal elasticity theory. Wang *et al*. (2019) extended the Chebyshev–Ritz based method in order to present the numerical results for static bending analysis of the graphene nanoplatelets reinforced nanocomposite plate using the virtual work principle. They discussed on the impact of graphene nanoplatelets distribution and amount as well as nanofiller characteristics on the deformation characteristics of the nanocomposite plate. Stability-based analysis of the carbon nanotube and carbon fiber reinforced nanocomposite plate was studied using an adopted size-capturing theory based on the Hamilton principle. After constituting the behavioral relations using the homogenization schemes, the numerical results were explored using the analytical approach in order to trace the impact of the filler and nano scale characteristics on the stability characteristics. More works on the material production are available in the literature works such as (Bai *et al*. 2020, 2022, Bao *et al*. 2024, Cao *et al*. 2024, Chen *et al*. 2023). The novel intelligent materials can be used in the control of systems and structures (Chu *et al*. 2021, 2025, Ding and Zhou 2022, Dong *et al*. 2025, Du *et al*. 2024). Jafari Mehrabadi *et al*. (2012) investigated impact of straight and inclined carbon nanotubes on the stability responses of the nanocomposite plate subjected to uniaxial/biaxial loading based on Mindlin's plate as well as first order shear defomation theories and Hamilton's principle. A large parametric analysis for investigating the impact of the reinforcement characteristics was provided in detail.

Investigating application of novel composite materials and new nanofillers are developed in the recent works (Li *et al*. 2024 a, b, Luo *et al*. 2024, Luo and Dong 2024, Lv *et al*. 2024a). They investigated impact of different combination of the boundary conditions on the vibrational analysis of the composite plate reinforced with nano scale reinforcement in nanotube and nanofiller configurations. It is developed Navier's technique for free vibration analysis of a sandwich plate integrated with two nanocomposite reinforced composite plate, where the homogenization scheme was applied based on Eshelby Mori Tanaka scheme. They presented a review paper on the nanocomposite structures and materials and its application in novel structures and systems. They discussed on the impact of various size-capturing theories and homogenization schemes for analysis of the nanocomposite structures and systems. He *et al*. (2021) presented an analytical work for investigating the bending responses of nanocomposite sandwich circular and annular plate using the hybrid modeling and theories. The solution was provided using the state space version of the differential quadrature method. A comprehensive investigation on the singular point was provided in the analysis. They studied bending and free vibration responses of a spherical shell reinforced with various distributions of graphene nanoplatelets subjected to mechanical loads using a general three dimensional elasticity solution method. The Eshelby-Mori-Tanaka methodology was used for investigating the thermal and mechanical dynamic behavior of the nano-composite sandwich plate subjected to thermomechanical loads. The pre thermal and mechanical loads were accounted in the external work expression using the constitutive relations. The kinematic modeling was accounted based on the higher order modeling.

Some works provided a detailed dynamic/stability analysis on the nanocomposite plate enriched by carbon nanotubes using a refined version of shear deformation theory in order to satisfy zero out of plane shear strains. The copper matrix may be used as the matrix in the novel structural elements (Feng *et al*. 2024, Gao *et al*. 2017, 2020, Han *et al*. 2025, Hou *et al*. 2025). Authors used the homogenization scheme for providing the overall material properties with changes of the material characteristics. Mehar and Panda (2018) prepared a computer simulation-based analysis as well as computer package analysis on the stress and deformation analysis of the nancarbon reinforced nanocomposite plate. The results were evaluated using the theoretical, numerical and experimental analyses and the efficiency of them has been evaluated with changes of various parameters. There are some analytical methods for solution of the governing equations of some problem such as suspension system and novel structures (Ji *et al*. 2023, Li *et al*. 2020, 2021 a, b, c). Shen (2009) employed a novel mathematical method for investigating the nonlinear behavior of a nanocomposite plate reinforced with single walled carbon nanotubes. The results were provided based on new version of perturbation technique with considering von Karman version of nonlinear strain components. a detailed parametric analysis on the impact of thermal loads and reinforcement content was performed. One can arrive at some analytical methods for derivation and analytical procedure of the governing equations of some problem such as control systems and innovative materials (Li *et al*. 2019 a, b, c, 2022 a, b). Furthermore, they studied the impact of elastic foundation characteristics on the dynamic/static responses of the nanocomposite reinforced plate with four distributions of the reinforcement using the shear deformable based kinematic model (Liu *et al*. 2022b).

Thai *et al*. (2019) presented a four variable kinematic based formulation in order to present deformation, stability and free vibration analyses of graphene nanoplatelets reinforced plate using the NURBS-based formulation. The various homogenization and mixture rules were employed for investigating the overall material properties of the nanocomposite structure. A curvilinear-based kinematic model was employed for static and dynamic analysis of the graphene nanoplatelet reinforced double curved shell by Wang *et al*. (2018), in which the overall material properties were evaluated using the micromechanical models in the Halpin-Tsai format and rule of mixture for various material properties. They employed finite element approach in hierarchical format for investigating the impact of carbon

nanotube reinforcement on the various analyses of the nanocomposite plate including buckling, vibrational characteristics and static bending responses. The main novelty of the paper was accounting the impact of van der Waals interaction on the assumed responses. They investigated impact of thermal and mechanical loads on the static results of shear deformable modeled graded plates resting on non-uniform foundation. Higher order deformability was accounted for the displacement field using a novel shape function in order to apply more accurate variation in shear strain components. They applied a novel three-dimensional theory in quasi form for transient analysis of a graphene nanoplatelets reinforced composite plate subjected to liquid medium. After derivation of the governing motion equations, the artificial neural network was applied to investigate impact of various parameters such as graphene content and various distributions on the natural frequencies responses. Guo *et al*. (2019) developed deep collocation approach for the Kirchhoff modeled plate in bending deformation. Zhuang *et al*. (2021) studied static, dynamic and buckling analyses of the Kirchhoff plate using the deep autoencoder scheme. Samaniego *et al*. (2020) developed an energy based approach for solution of the partial differential equations based on the machine learning. Uncertainties in the input parameters are recently accounted in the works to present a general sensitivity analysis on the impact of each parameter on the responses (Nam *et al*. 2019, Cheng *et al*. 2024). There are some review works on the graphene based structures and 2D nanomaterials in the literature works (Ghosh *et al*. 2023, Das *et al*. 2024).

Ansari *et al*. (2020) investigated the impact of geometric nonlinearity on the static responses of the graphene nanoplatelets reinforced composite plate with cutout of various shapes. The porosity was accounted for the material distribution and the Gaussian random-field was applied for investigating the effective material characteristics. The problem was analyzed and solved using the variational form of differential quadrature method and finite element formulation. They investigated impact of thermal loads and various foundation characteristics on the vibrational and bending responses of the higher deformable nanocomposite plate using the computational method of generalized differential quadrature method. Sensitivity of the responses with changes of graphene nanoplatelets characteristics and foundation parameter was presented using the parametric analysis. Zhao *et al*. (2017) investigated the impact of trapezoidal shape of the plate on the static/bending responses of graphene nanoplatelets reinforced nanocomposite plate with various distributions of porosity. The solution procedure was developed using finite element approach in which the Halpin-Tsai micromechanical model was applied for estimation of the effective material properties. A parametric investigation on the impact of various distributions and graphene amount was presented. They developed a multi scale finite element approach for vibrational and stability responses of nanocomposite plate enriched by carbon nanotubes. They modeled the chemical interactions using some mathematical modeling. García-Macías *et al*. (2018) employed some novel models for investigating the impact of agglomeration characteristics of carbon nanotubes on the structural static/dynamic responses of the nanocomposite plate. The sensitivity of the responses was accounted on the static/dynamic responses of the nanocomposite plate. Liu *et al*. (2019) developed an elasticity-based formulation in three-dimensional framework in order to study bending responses of graphene nanoplatelets reinforced composite annular plate using the state-space formulation and differential quadrature method. They discussed on the selection of the best configuration of the reinforcement on the dynamic/static responses. They presented a numerical investigation on the improvement of the mechanical behavior and responses of the nanocomposite sandwich plate using a mesh free analysis. Molecular dynamic and moving least square approaches were developed for estimation of the overall material properties and extending the mesh free approach. Song *et al*. (2018) extended a lower order shear deformable model for investigating the bending and buckling responses of the multi-layered composite plate, where the overall material characteristics were evaluated using the micromechanical-based models. Zghal *et al*. (2018) studied effect of a higher order shearing kinematic model for investigating the nonlinear responses of the nanotube reinforced shell with various distributions and functionalities. After presentation of convergence study, an investigation on the impact of various patterns of reinforcement and its amount on the responses was provided. Feng *et al*. (2017) presented an analytical work for investigating the impact of geometric nonlinearity and graphene nanoplatelets patterns on the large deflection bending results of the nanocomposite reinforced beam using the micromechanical model and Ritz method. They discussed on the impact of various nanofillers dispersion and its effect on the overall stiffness of the nanocomposite beam.

A comprehensive review on the analysis of shear deformable materials, structures and nanocomposite structures was presented in the literature review section. It is concluded that deformation analysis of nanocomposite reinforced double curved shell including graphene origami nanofillers is necessary for designer and engineers. In this paper, after presentation of the necessary relations for the overall material characteristics of the graphene origami reinforced materials using the experimental and statistical relations of the literature, the analytical formulation is presented based on the virtual work principle and shear deformable-based kinematic relations. The results will be presented using the analytical method in order to investigate the influence of important parameters of the nanocomposite and loading characteristics on the deformation and results.

2. Governing equations

Variational-based method is developed in the curvilinear coordinate system to derive the governing equations of the deformation and strain behavior for a graphene origami-based nanocomposite. The kinematic relations are developed based on the first order shear deformation theory. It is assumed that graphene origami is uniformly dispersed along the thickness direction. The shell is subjected to uniform

temperature rising. To arrive at the governing equations, one should complete strain energy and external work in the curvilinear coordinate system. The strain energy variation is assumed as follows (Arefi and Rahimi, 2010, 2011, 2012a, b, c, Rahimi *et al*. 2012, Arefi *et al*. 2012, 2016, 2019, 2020, 2021, Arefi and Kiani 2020, Arefi and Mohammad-Rezaei Bidgoli 2020, Arefi 2016, 2018, 2020, Arefi and Zenkour 2016a, b, 2017a, b, c, 2018 a, b, 2019 a, b, Mohammad *et al*. 2019, Lori *et al*. 2021, Zhang *et al*. 2023, Mohammadimehr *et al*. 2016, Arefi and Allam 2015):

$$U = \int_{\mathcal{Y}=0}^{\mathcal{Y}_1}\int_{\mathcal{X}=0}^{\mathcal{X}_1}\int_{\mathcal{Z}=-0.5h}^{\mathcal{Z}=+0.5h}[\sigma_{\mathcal{X}}\delta\varepsilon_{\mathcal{X}} + \sigma_{\mathcal{Y}}\delta\varepsilon_{\mathcal{Y}} + \sigma_{\mathcal{X}\mathcal{Y}}\delta\gamma_{\mathcal{X}\mathcal{Y}} + \sigma_{\mathcal{X}\mathcal{Z}}\delta\gamma_{\mathcal{X}\mathcal{Z}} + \sigma_{\mathcal{Y}\mathcal{Z}}\delta\gamma_{\mathcal{Y}\mathcal{Z}}]\, d\mathcal{Z}\left(1+\frac{\mathcal{Z}}{\mathcal{R}_{\mathcal{X}}}\right)d\mathcal{X}\left(1+\frac{\mathcal{Z}}{\mathcal{R}_{\mathcal{Y}}}\right)d\mathcal{Y} \quad (1)$$

In which, σ_{ij}, and ε_i, γ_{ij} are stress and strain component and $\mathcal{R}_{\mathcal{X}}, \mathcal{R}_{\mathcal{Y}}$ are radii of curvature. In addition, the external work should be accounted to complete variational-based formulation. The external work is included may be composed of transverse loads, foundation's reaction and in-plane multi-field loading. In this work, the uniform transverse load and in-plane thermal load is accounted and therefore the external work is assumed as follows (Tlidji *et al*. 2022, Madenci *et al*. 2023, Kumar *et al*. 2021, Din *et al*. 2023, Zhou *et al*. 2020, Kadiri *et al*. 2024, Sekkak *et al*. 2024):

$$\delta W = \int\{\mathcal{W}_{\mathcal{X}}^{T} + \mathcal{W}_{\mathcal{Y}}^{T} + \mathcal{W}_{Transverse}^{M}\}R_{\xi}R_{\zeta}\delta w d\mathcal{X}d\mathcal{Y} \quad (2)$$

In which $\mathcal{W}_{\mathcal{X}}^{T}$, $\mathcal{W}_{\mathcal{Y}}^{T}$ are pre-thermal loads along the $\mathcal{X}$, directions, respectively and $\mathcal{W}_{Transverse}^{M}$ is uniform transvers loadings. The first two terms will be obtained after definition of the resultant components.

Computation of strain energy and external work defined in Eqs. (1, 2) can be completed after definition of the kinematic relations. This paper uses a lower order deformable model as follows:

$$\begin{aligned}\mathcal{U}_{\mathcal{X}} &= \left(1+\frac{\mathcal{Z}}{\mathcal{R}_{\mathcal{X}}}\right)\mathcal{U} + \mathcal{Z}\phi_{\mathcal{X}},\\ \mathcal{U}_{\mathcal{Y}} &= \left(1+\frac{\mathcal{Z}}{\mathcal{R}_{\mathcal{Y}}}\right)\mathcal{V} + \mathcal{Z}\phi_{\mathcal{Y}},\\ \mathcal{U}_{\mathcal{Z}} &= \mathcal{w}\end{aligned} \quad (3)$$

In which the general deformation along three orthogonal coordinates are denoted with $\mathcal{U}_{\mathcal{X}}, \mathcal{U}_{\mathcal{Y}}, \mathcal{U}_{\mathcal{Z}}$, the middle surface deformations are denoted with $\mathcal{U}, \mathcal{V}, \mathcal{w}$ and the rotation components are denoted with $\phi_{\mathcal{X}}, \phi_{\mathcal{Y}}$ about the $\mathcal{Y}, \mathcal{X}$ directions, and the radius of curvature with $\mathcal{R}_{\mathcal{X}}, \mathcal{R}_{\mathcal{Y}}$.

Using the kinematic relations, one can use the continuum relations in curvilinear coordinate system as follows (Zhou *et al*. 2017, 2018, Ni *et al*. 2024, Tian *et al*. 2023, Shi *et al*. 2024):

$$\begin{aligned}\varepsilon_{\mathcal{X}} &= \frac{1}{\mathcal{R}_{\mathcal{X}}\left(1+\frac{\mathcal{Z}}{\mathcal{R}_{\mathcal{X}}}\right)}\frac{\partial\mathcal{U}}{\partial\mathcal{X}} + \frac{\mathcal{w}}{\mathcal{R}_{\mathcal{X}}} + \frac{\mathcal{Z}}{\mathcal{R}_{\mathcal{X}}\left(1+\frac{\mathcal{Z}}{\mathcal{R}_{\mathcal{X}}}\right)}\frac{\partial\phi_{\mathcal{X}}}{\partial\mathcal{X}},\\ \varepsilon_{\mathcal{Y}} &= \frac{1}{\mathcal{R}_{\mathcal{Y}}\left(1+\frac{\mathcal{Z}}{\mathcal{R}_{\mathcal{Y}}}\right)}\frac{\partial\mathcal{V}}{\partial\mathcal{Y}} + \frac{\mathcal{w}}{\mathcal{R}_{\mathcal{Y}}} + \frac{\mathcal{Z}}{\mathcal{R}_{\mathcal{Y}}\left(1+\frac{\mathcal{Z}}{\mathcal{R}_{\mathcal{Y}}}\right)}\frac{\partial\phi_{\mathcal{Y}}}{\partial\mathcal{Y}},\\ \gamma_{\mathcal{Y}\mathcal{Z}} &= \phi_{\mathcal{Y}} + \frac{1}{\mathcal{R}_{\mathcal{Y}}\left(1+\frac{\mathcal{Z}}{\mathcal{R}_{\mathcal{Y}}}\right)}\frac{\partial\mathcal{w}}{\partial\mathcal{Y}} - \frac{\mathcal{V}}{R_{\mathcal{Y}}},\end{aligned} \quad (4)$$

$$U = \int_{\mathcal{Y}=0}^{\mathcal{Y}_1}\int_{\mathcal{X}=0}^{\mathcal{X}_1}\int_{\mathcal{Z}=-0.5h}^{\mathcal{Z}=+0.5h}\left\{\begin{array}{l}\sigma_{\mathcal{X}}\left\{\frac{1}{\mathcal{R}_{\mathcal{X}}\left(1+\frac{\mathcal{Z}}{\mathcal{R}_{\mathcal{X}}}\right)}\frac{\partial\delta\mathcal{U}}{\partial\mathcal{X}} + \frac{\delta\mathcal{w}}{\mathcal{R}_{\mathcal{X}}} + \frac{\mathcal{Z}}{\mathcal{R}_{\mathcal{X}}\left(1+\frac{\mathcal{Z}}{\mathcal{R}_{\mathcal{X}}}\right)}\frac{\partial\delta\phi_{\mathcal{X}}}{\partial\mathcal{X}}\right\}\\ \sigma_{\mathcal{Y}}\left\{\frac{1}{\mathcal{R}_{\mathcal{Y}}\left(1+\frac{\mathcal{Z}}{\mathcal{R}_{\mathcal{Y}}}\right)}\frac{\partial\delta\mathcal{V}}{\partial\mathcal{Y}} + \frac{\delta\mathcal{w}}{\mathcal{R}_{\mathcal{Y}}} + \frac{\mathcal{Z}}{\mathcal{R}_{\mathcal{Y}}\left(1+\frac{\mathcal{Z}}{\mathcal{R}_{\mathcal{Y}}}\right)}\frac{\partial\delta\phi_{\mathcal{Y}}}{\partial\mathcal{Y}}\right\}\\ +\sigma_{\mathcal{X}\mathcal{Y}}\left\{\begin{array}{l}\frac{1}{\mathcal{R}_{\mathcal{X}}\left(1+\frac{\mathcal{Z}}{\mathcal{R}_{\mathcal{X}}}\right)}\frac{\partial\delta\mathcal{V}}{\partial\mathcal{X}} + \frac{1}{\mathcal{R}_{\mathcal{Y}}\left(1+\frac{\mathcal{Z}}{\mathcal{R}_{\mathcal{Y}}}\right)}\frac{\partial\delta\mathcal{U}}{\partial\mathcal{Y}} +\\ \mathcal{Z}\left[\begin{array}{l}\frac{1}{\mathcal{R}_{\mathcal{X}}\left(1+\frac{\mathcal{Z}}{\mathcal{R}_{\mathcal{X}}}\right)}\frac{\partial\delta\phi_{\mathcal{Y}}}{\partial\mathcal{X}} + \frac{1}{\mathcal{R}_{\mathcal{Y}}\left(1+\frac{\mathcal{Z}}{\mathcal{R}_{\mathcal{Y}}}\right)}\frac{\partial\delta\phi_{\mathcal{X}}}{\partial\mathcal{Y}}\\ +\frac{1}{2}\left(\frac{1}{\mathcal{R}_{\mathcal{X}}}-\frac{1}{\mathcal{R}_{\mathcal{Y}}}\right)\left(\frac{1}{\mathcal{R}_{\mathcal{X}}\left(1+\frac{\mathcal{Z}}{\mathcal{R}_{\mathcal{X}}}\right)}\frac{\partial\delta\mathcal{V}}{\partial\mathcal{X}} - \frac{1}{\mathcal{R}_{\mathcal{Y}}\left(1+\frac{\mathcal{Z}}{\mathcal{R}_{\mathcal{Y}}}\right)}\frac{\partial\delta\mathcal{U}}{\partial\mathcal{Y}}\right)\end{array}\right]\end{array}\right\}\\ +\sigma_{\mathcal{X}\mathcal{Z}}\left\{\delta\phi_{\mathcal{Y}} + \frac{1}{\mathcal{R}_{\mathcal{Y}}\left(1+\frac{\mathcal{Z}}{\mathcal{R}_{\mathcal{Y}}}\right)}\frac{\partial\delta\mathcal{w}}{\partial\mathcal{Y}} - \frac{\delta\mathcal{V}}{R_{\mathcal{Y}}}\right\}\\ +\sigma_{\mathcal{Y}\mathcal{Z}}\left\{\delta\phi_{\mathcal{X}} + \frac{1}{\mathcal{R}_{\mathcal{X}}\left(1+\frac{\mathcal{Z}}{\mathcal{R}_{\mathcal{X}}}\right)}\frac{\partial\delta\mathcal{w}}{\partial\mathcal{X}} - \frac{\delta\mathcal{U}}{R_{\mathcal{X}}}\right\}\end{array}\right\}d\mathcal{Z}d \quad (5)$$

$$\gamma_{\mathcal{X}\mathcal{Z}} = \phi_{\mathcal{X}} + \frac{1}{\mathcal{R}_{\mathcal{X}}\left(1+\frac{\mathcal{Z}}{\mathcal{R}_{\mathcal{X}}}\right)}\frac{\partial \mathcal{w}}{\partial \mathcal{X}} - \frac{\mathcal{U}}{R_{\mathcal{X}}}$$

$$\gamma_{\mathcal{X}\mathcal{Y}} = \frac{1}{\mathcal{R}_{\mathcal{X}}\left(1+\frac{\mathcal{Z}}{\mathcal{R}_{\mathcal{X}}}\right)}\frac{\partial \mathcal{V}}{\partial \mathcal{X}} + \frac{1}{\mathcal{R}_{\mathcal{Y}}\left(1+\frac{\mathcal{Z}}{\mathcal{R}_{\mathcal{Y}}}\right)}\frac{\partial \mathcal{U}}{\partial \mathcal{Y}} + \mathcal{Z}\left[\begin{array}{c} \frac{1}{\mathcal{R}_{\mathcal{X}}\left(1+\frac{\mathcal{Z}}{\mathcal{R}_{\mathcal{X}}}\right)}\frac{\partial \phi_{\mathcal{Y}}}{\partial \mathcal{X}} + \frac{1}{\mathcal{R}_{\mathcal{Y}}\left(1+\frac{\mathcal{Z}}{\mathcal{R}_{\mathcal{Y}}}\right)}\frac{\partial \phi_{\mathcal{X}}}{\partial \mathcal{Y}} \\ +\frac{1}{2}\left(\frac{1}{\mathcal{R}_{\mathcal{X}}} - \frac{1}{\mathcal{R}_{\mathcal{Y}}}\right)\left(\frac{1}{\mathcal{R}_{\mathcal{X}}\left(1+\frac{\mathcal{Z}}{\mathcal{R}_{\mathcal{X}}}\right)}\frac{\partial \mathcal{V}}{\partial \mathcal{X}} - \frac{1}{\mathcal{R}_{\mathcal{Y}}\left(1+\frac{\mathcal{Z}}{\mathcal{R}_{\mathcal{Y}}}\right)}\frac{\partial \mathcal{U}}{\partial \mathcal{Y}}\right) \end{array}\right], \quad (6)$$

Substitution of the variation version of the strain components into the strain energy variation yields to Eq. (5) above.

In order to present strain energy in more simple form, one can define the resultant components in the following format (Jermsittiparsert *et al*. 2020, Ma *et al*. 2023, Peng *et al*. 2023, Song *et al*. 2024, Shi *et al*. 2022, Wu and Habibi 2022, Xiao *et al*. 2024, Yin *et al*. 2024, Zhu *et al*. 2022, Zhiqiang *et al*. 2024, Guo *et al*. 2024, Huo *et al*. 2021, Liang *et al*. 2024 a, Li *et al*. 2022c, 2024c, Lu *et al*. 2023, Liu *et al*. 2022a, Jin *et al*. 2024, Ge *et al*. 2023):

$$\begin{aligned}
\{\mathcal{R}^1_{\mathcal{X}}, \mathcal{R}^2_{\mathcal{X}}, \mathcal{R}^3_{\mathcal{X}}\} &= \int_{-h/2}^{+h/2} \sigma_{\mathcal{X}}\left(1+\frac{\mathcal{Z}}{\mathcal{R}_{\mathcal{Y}}}\right)\left\{1, \left(1+\frac{\mathcal{Z}}{\mathcal{R}_{\mathcal{X}}}\right), \mathcal{Z}\right\} d\mathcal{Z}. \\
\{\mathcal{R}^4_{\mathcal{X}}, \mathcal{R}^5_{\mathcal{X}}, \mathcal{R}^6_{\mathcal{X}}\} &= \int_{-h/2}^{+h/2} \sigma_{\mathcal{Y}}\left(1+\frac{\mathcal{Z}}{\mathcal{R}_{\mathcal{X}}}\right)\left\{1, \left(1+\frac{\mathcal{Z}}{\mathcal{R}_{\mathcal{Y}}}\right), \mathcal{Z}\right\} d\mathcal{Z}. \\
\{\mathcal{R}^7_{\mathcal{Y}\mathcal{Z}}, \mathcal{R}^8_{\mathcal{Y}\mathcal{Z}}\} &= \int_{-h/2}^{+h/2} \tau_{\mathcal{Y}\mathcal{Z}}\left(1+\frac{\mathcal{Z}}{\mathcal{R}_{\mathcal{X}}}\right)\left\{1, \left(1+\frac{\mathcal{Z}}{\mathcal{R}_{\mathcal{Y}}}\right)\right\} d\mathcal{Z}. \\
\{\mathcal{R}^9_{\mathcal{X}\mathcal{Z}}, \mathcal{R}^{10}_{\mathcal{X}\mathcal{Z}}\} &= \int_{-h/2}^{+h/2} \tau_{\mathcal{X}\mathcal{Z}}\left(1+\frac{\mathcal{Z}}{\mathcal{R}_{\mathcal{Y}}}\right)\left\{1, \left(1+\frac{\mathcal{Z}}{\mathcal{R}_{\mathcal{X}}}\right)\right\} d\mathcal{Z} \\
\{\mathcal{R}^{11}_{\mathcal{X}\mathcal{Y}}, \mathcal{R}^{12}_{\mathcal{X}\mathcal{Y}}\} &= \int_{-h/2}^{+h/2} \tau_{\mathcal{X}\mathcal{Y}}\left(1+\frac{\mathcal{Z}}{\mathcal{R}_{\mathcal{Y}}}\right)\{1, \mathcal{Z}\} d\mathcal{Z}. \\
\{\mathcal{R}^{13}_{\mathcal{Y}\mathcal{X}}, \mathcal{R}^{14}_{\mathcal{Y}\mathcal{X}}\} &= \int_{-h/2}^{+h/2} \tau_{\mathcal{Y}\mathcal{X}}\left(1+\frac{\mathcal{Z}}{\mathcal{R}_{\mathcal{X}}}\right)\{1, \mathcal{Z}\} d\mathcal{Z}
\end{aligned} \quad (7)$$

Using Eq. (6), one can arrive at more simple form of strain energy variation as follows (Yang *et al*. 2024, Samadzadeh *et al*. 2024, 2018, Arefi and Kiani 2020, Arefi and Bidgoli 2019)

To complete resultant components, one can use the constitutive relations with accounting the thermal strain components as follows (Wang *et al*. 2024c, d, e, Liang *et al*. 2024b, Cong *et al*. 2024)

$$\begin{aligned}
\sigma_{\mathcal{X}} &= \frac{\mathbb{E}}{1-\mathcal{v}^2}\{\varepsilon_{\mathcal{X}} - \alpha_{eff}\mathcal{T} + \mathcal{v}(\varepsilon_{\mathcal{Y}} - \alpha\mathcal{T})\} \\
\sigma_{\mathcal{Y}} &= \frac{\mathbb{E}}{1-\mathcal{v}^2}\{\varepsilon_{\mathcal{Y}} - \alpha_{eff}\mathcal{T} + \mathcal{v}(\varepsilon_{\mathcal{X}} - \alpha\mathcal{T})\} \\
\sigma_{\mathcal{Y}\mathcal{Z}} &= \hbar_s \frac{\mathbb{E}}{2(1+\mathcal{v})}\gamma_{\mathcal{Y}\mathcal{Z}} \\
\sigma_{\mathcal{X}\mathcal{Z}} &= \hbar_s \frac{\mathbb{E}}{2(1+\mathcal{v})}\gamma_{\mathcal{X}\mathcal{Z}} \\
\sigma_{\mathcal{X}\mathcal{Y}} &= \frac{\mathbb{E}}{2(1+\mathcal{v})}\gamma_{\mathcal{X}\mathcal{Y}}
\end{aligned} \quad (8)$$

In which the overall modulus of elasticity and Poisson's ratio are defined with $\mathbb{E}, \mathcal{v}$ respectively. furthermore, the overall heat expansion coefficient is defined with α. The shear correction factor is denoted with $\hbar_s$. The effective modulus of elasticity, Poisson's ratio and heat expansion coefficient are estimated as follows (Zhao *et al*. 2022, Zhang *et al*. 2024d, Zha and Zhang 2024, Shen *et al*. 2024, Long *et al*. 2024):

$$\begin{aligned}
\mathbb{E} &= \frac{1+2\frac{\frac{\mathbb{E}_G}{\mathbb{E}_C}-1}{\frac{\mathbb{E}_G}{\mathbb{E}_C}+\xi}\frac{l_G}{t_G}V_G}{1-2\frac{l_G}{t_G}V_G}\mathbb{E}_C\left(1.11 - 1.22V_G - 0.134\left(\frac{\mathcal{T}}{\mathcal{T}_0}\right) + 0.559V_G\left(\frac{\mathcal{T}}{\mathcal{T}_0}\right) - 5.5V_GH_G + 38V_G^2H_G - 20.6V_G^2H_G^2\right), \\
\mathcal{v} &= \left(\mathcal{v}_GV_G + \mathcal{v}_C(1-V_G)\right)\left(1.01 - 1.43V_G + 0.165\left(\frac{\mathcal{T}}{\mathcal{T}_0}\right) - 1.1V_GH_G\left(\frac{\mathcal{T}}{\mathcal{T}_0}\right) - 16.8V_GH_G + 16V_G^2H_G^2\right), \\
\alpha &= \left(\alpha_GV_G + \alpha_C(1-V_G)\right)\left(0.794 - 16.8V_G^2 - 0.0279\left(\frac{\mathcal{T}}{\mathcal{T}_0}\right)^2 + 0.182(1+V_G)\left(\frac{\mathcal{T}}{\mathcal{T}_0}\right)\right)
\end{aligned} \quad (9)$$

in which, $\mathbb{E}_G$, $\mathbb{E}_C$ are modulus of elasticity of graphene origami nano material and Cu matrix, respectively, and l_{Gr}, t_{Gr} are length and thickness of graphene origami nano material, respectively. V_C, V_G are used as content percentage of Cu as matrix and graphene origami auxetic metamaterial as reinforcement. Furthermore, (ν_G, ν_C) and (α_G, α_C) are Poisson's ratio and hear expansion coefficients of origami and Cu matrix, respectively.

An update version of Eq.7 and employing Eq. (2) yields to final governing equations as follows (Zhang *et al*. 2024 a, b, Zhang *et al*. 2025 a, b):

$$\begin{aligned}
&\frac{\partial}{\partial \mathcal{X}}\left(\frac{\mathcal{R}^1_{\mathcal{X}}}{R_{\mathcal{X}}}\right) + \frac{\partial}{\partial \mathcal{Y}}\left(\frac{\mathcal{R}^{13}_{\mathcal{Y}\mathcal{X}}}{R_{\mathcal{Y}}}\right) + \frac{\mathcal{R}^{10}_{\mathcal{X}\mathcal{Z}}}{R_{\mathcal{X}}} - \frac{1}{2}\left(\frac{1}{R_{\mathcal{X}}} - \frac{1}{R_{\mathcal{Y}}}\right)\frac{\partial}{\partial \mathcal{Y}}\left(\frac{\mathcal{R}^{14}_{\mathcal{Y}\mathcal{X}}}{R_{\mathcal{Y}}}\right) = 0, \\
&\frac{\partial}{\partial \mathcal{X}}\left(\frac{\mathcal{R}^3_{\mathcal{X}}}{R_{\mathcal{X}}}\right) - \mathcal{R}^{10}_{\mathcal{X}\mathcal{Z}} + \frac{\partial}{\partial \mathcal{Y}}\left(\frac{\mathcal{R}^{14}_{\mathcal{Y}\mathcal{X}}}{R_{\mathcal{Y}}}\right) = 0, \\
&\frac{\partial}{\partial \mathcal{Y}}\left(\frac{\mathcal{R}^4_{\mathcal{X}}}{\mathcal{R}_{\mathcal{Y}}}\right) + \frac{\partial}{\partial \xi}\left(\frac{\mathcal{R}^{11}_{\mathcal{X}\mathcal{Y}}}{R_{\xi}}\right) + \frac{\mathcal{R}^8_{\mathcal{Y}\mathcal{Z}}}{R_{\mathcal{Y}}} + \frac{1}{2}\left(\frac{1}{R_{\xi}} - \frac{1}{R_{\mathcal{Y}}}\right)\frac{\partial}{\partial \mathcal{X}}\left(\frac{\mathcal{R}^{12}_{\mathcal{X}\mathcal{Y}}}{R_{\mathcal{X}}}\right) = 0, \\
&\frac{\partial}{\partial \mathcal{Y}}\left(\frac{\mathcal{R}^6_{\mathcal{X}}}{\mathcal{R}_{\mathcal{Y}}}\right) - \mathcal{R}^8_{\mathcal{Y}\mathcal{Z}} + \frac{\partial}{\partial \mathcal{X}}\left(\frac{\mathcal{R}^{12}_{\mathcal{X}\mathcal{Y}}}{R_{\mathcal{X}}}\right) = 0, \\
&-\frac{\mathcal{R}^2_{\mathcal{X}}}{R_{\mathcal{X}}} - \frac{\mathcal{R}^5_{\mathcal{X}}}{\mathcal{R}_{\mathcal{Y}}} + \frac{\partial}{\partial \mathcal{Y}}\left(\frac{\mathcal{R}^7_{\mathcal{Y}\mathcal{Z}}}{\mathcal{R}_{\mathcal{Y}}}\right) + \frac{\partial}{\partial \mathcal{X}}\left(\frac{\mathcal{R}^9_{\mathcal{X}\mathcal{Z}}}{R_{\mathcal{X}}}\right) - \frac{\mathbb{N}_{\xi}{}^{\mathrm{T}}}{R_{\xi}^2}\frac{\partial^2 \mathcal{w}}{\partial \mathcal{X}^2} - \frac{\mathbb{N}_{\zeta}{}^{\mathrm{T}}}{R_{\mathcal{Y}}^2}\frac{\partial^2 \mathcal{w}}{\partial \mathcal{Y}^2} = q\left(1+\frac{h}{2R_{\mathcal{X}}}\right)\left(1+\frac{h}{2\mathcal{R}_{\mathcal{Y}}}\right),
\end{aligned} \quad (10)$$

In which, one can arrive at the resultant components in the following format (Deng *et al*. 2024, 2025, Ye *et al*.

2025, Wei *et al*. 2024, Ren *et al*. 2025):

$$\begin{Bmatrix}\mathcal{R}_X^1\\ \mathcal{R}_X^2\\ \mathcal{R}_X^3\\ \mathcal{R}_X^4\\ \mathcal{R}_X^5\\ \mathcal{R}_X^6\end{Bmatrix}=\begin{bmatrix}\mathfrak{V}_1 & \mathfrak{V}_2 & \mathfrak{V}_3 & \mathfrak{V}_4 & \mathfrak{V}_5 & \mathfrak{V}_6\\ \mathfrak{V}_8 & \mathfrak{V}_9 & \mathfrak{V}_{10} & \mathfrak{V}_{11} & \mathfrak{V}_{12} & \mathfrak{V}_{13}\\ \mathfrak{V}_{15} & \mathfrak{V}_{16} & \mathfrak{V}_{17} & \mathfrak{V}_{18} & \mathfrak{V}_{19} & \mathfrak{V}_{20}\\ \mathfrak{V}_4 & \mathfrak{V}_5 & \mathfrak{V}_6 & \mathfrak{V}_{22} & \mathfrak{V}_{23} & \mathfrak{V}_{24}\\ \mathfrak{V}_{11} & \mathfrak{V}_{12} & \mathfrak{V}_{13} & \mathfrak{V}_{25} & \mathfrak{V}_{26} & \mathfrak{V}_{27}\\ \mathfrak{V}_{18} & \mathfrak{V}_{19} & \mathfrak{V}_{20} & \mathfrak{V}_{28} & \mathfrak{V}_{29} & \mathfrak{V}_{30}\end{bmatrix}\begin{Bmatrix}\frac{\partial \mathcal{U}}{\partial X}\\ w\\ \frac{\partial \phi_X}{\partial X}\\ \frac{\partial \mathcal{V}}{\partial Y}\\ w\\ \frac{\partial \phi_Y}{\partial Y}\end{Bmatrix}+\begin{Bmatrix}\mathcal{R}_X^{1T}\\ \mathcal{R}_X^{2T}\\ \mathcal{R}_X^{3T}\\ \mathcal{R}_X^{4T}\\ \mathcal{R}_X^{5T}\\ \mathcal{R}_X^{6T}\end{Bmatrix}$$

$$\begin{Bmatrix}\mathcal{R}_{YZ}^7\\ \mathcal{R}_{YZ}^8\\ \mathcal{R}_{XZ}^9\\ \mathcal{R}_{XZ}^{10}\end{Bmatrix}=\begin{bmatrix}\mathfrak{V}_{31} & \mathfrak{V}_{32} & \mathfrak{V}_{33} & \mathfrak{V}_{34}\\ \mathfrak{V}_{39} & \mathfrak{V}_{40} & \mathfrak{V}_{41} & \mathfrak{V}_{42}\\ \mathfrak{V}_{35} & \mathfrak{V}_{36} & \mathfrak{V}_{37} & \mathfrak{V}_{38}\\ \mathfrak{V}_{43} & \mathfrak{V}_{44} & \mathfrak{V}_{45} & \mathfrak{V}_{46}\end{bmatrix}\begin{Bmatrix}\phi_Y\\ \frac{\partial w}{\partial Y}\\ -\mathcal{V}\\ -\frac{\partial w}{\partial Y}\end{Bmatrix} \tag{11}$$

$$\begin{Bmatrix}\mathcal{R}_{XY}^{11}\\ \mathcal{R}_{YX}^{13}\\ \mathcal{R}_{XY}^{12}\\ \mathcal{R}_{YX}^{14}\end{Bmatrix}=\begin{bmatrix}\mathfrak{V}_{47} & \mathfrak{V}_{48} & \mathfrak{V}_{49} & \mathfrak{V}_{50} & \mathfrak{V}_{51} & \mathfrak{V}_{52}\\ \mathfrak{V}_{53} & \mathfrak{V}_{54} & \mathfrak{V}_{55} & \mathfrak{V}_{56} & \mathfrak{V}_{57} & \mathfrak{V}_{58}\\ \mathfrak{V}_{59} & \mathfrak{V}_{60} & \mathfrak{V}_{61} & \mathfrak{V}_{62} & \mathfrak{V}_{63} & \mathfrak{V}_{64}\\ \mathfrak{V}_{65} & \mathfrak{V}_{66} & \mathfrak{V}_{67} & \mathfrak{V}_{68} & \mathfrak{V}_{69} & \mathfrak{V}_{70}\end{bmatrix}\begin{Bmatrix}\frac{\partial \mathcal{V}}{\partial X}\\ \frac{\partial \mathcal{U}}{\partial Y}\\ \frac{\partial \phi_Y}{\partial X}\\ \frac{\partial \phi_X}{\partial Y}\\ \frac{\partial \mathcal{V}}{\partial X}\\ \frac{\partial \mathcal{U}}{\partial Y}\end{Bmatrix}$$

The external loads pre-defined in Eq. (2) are now computed as (Xie *et al*. 2023, 2024a, b, Xu *et al*. 2021, Yu *et al*. 2024b): $\mathcal{W}_X^T=\frac{\mathcal{R}_X^{1T}}{R_X^2}\frac{\partial^2 w}{\partial X^2}, \mathcal{W}_Y^T=\frac{\mathcal{R}_X^{4T}}{R_Y^2}\frac{\partial^2 w}{\partial Y^2}$.

Final update format of the governing equations in terms of primary unknown functions are derived as follows (Zhao *et al*. 2019, Shen *et al*. 2025, Sun *et al*. 2024, Wang *et al*. 2024b, 2025):

$$\begin{aligned}&\frac{\mathfrak{V}_1}{R_X}\frac{\partial^2 \mathcal{U}}{\partial X^2}+\left(\frac{\chi(\mathfrak{V}_{70}-\mathfrak{V}_{66})+\mathfrak{V}_{54}-\mathfrak{V}_{58}}{\mathcal{R}_Y}\right)\frac{\partial^2 \mathcal{U}}{\partial Y^2}-\frac{\mathfrak{V}_{45}}{R_X}u\\&+\frac{\mathfrak{V}_3}{R_X}\frac{\partial^2 \phi_X}{\partial X^2}+\left(\frac{\mathfrak{V}_{56}-\chi\mathfrak{V}_{68}}{\mathcal{R}_Y}\right)\frac{\partial^2 \phi_X}{\partial Y^2}+\frac{\mathfrak{V}_{43}}{R_X}\phi_X\\&+\left(\frac{\mathfrak{V}_4}{R_X}+\frac{\mathfrak{V}_{57}+\mathfrak{V}_{53}-\chi(\mathfrak{V}_{65}+\mathfrak{V}_{69})}{\mathcal{R}_Y}\right)\frac{\partial^2 \mathcal{V}}{\partial X\partial Y}\\&+\left(\frac{\mathfrak{V}_6}{R_X}+\frac{\mathfrak{V}_{55}-\chi\mathfrak{V}_{67}}{\mathcal{R}_Y}\right)\frac{\partial^2 \phi_Y}{\partial X\partial Y}+\left(\frac{\mathfrak{V}_5+\mathfrak{V}_2+\mathfrak{V}_{44}}{R_X}\right)\frac{\partial w}{\partial X}=0\end{aligned} \tag{12a}$$

$$\begin{aligned}&\frac{\mathfrak{V}_{15}}{R_X}\frac{\partial^2 \mathcal{U}}{\partial X^2}+\frac{(\mathfrak{V}_{66}-\mathfrak{V}_{70})}{\mathcal{R}_Y}\frac{\partial^2 \mathcal{U}}{\partial Y^2}+\mathfrak{V}_{45}\mathcal{U}+\frac{\mathfrak{V}_{17}}{R_X}\frac{\partial^2 \phi_X}{\partial X^2}\\&+\frac{\mathfrak{V}_{68}}{\mathcal{R}_Y}\frac{\partial^2 \phi_X}{\partial Y^2}-\mathfrak{V}_{43}\phi_X+\left(\frac{\mathfrak{V}_{65}+\mathfrak{V}_{69}}{\mathcal{R}_Y}+\frac{\mathfrak{V}_{18}}{R_X}\right)\frac{\partial^2 \mathcal{V}}{\partial X\partial Y}\\&+\left(\frac{\mathfrak{V}_{20}}{R_X}+\frac{\mathfrak{V}_{67}}{\mathcal{R}_Y}\right)\frac{\partial \phi_Y}{\partial X\partial Y}+\left(\frac{\mathfrak{V}_{19}+\mathfrak{V}_{16}}{R_X}-\mathfrak{V}_{44}\right)\frac{\partial w}{\partial X}=0\end{aligned} \tag{12b}$$

$$\begin{aligned}&\delta v:\left(\frac{\mathfrak{V}_4}{\mathcal{R}_Y}+\frac{(\mathfrak{V}_{60}-\mathfrak{V}_{64})\chi+\mathfrak{V}_{48}-\mathfrak{V}_{52}}{R_X}\right)\frac{\partial^2 \mathcal{U}}{\partial X\partial Y}\\&+\left(\frac{\mathfrak{V}_{50}+\chi\mathfrak{V}_{62}}{R_X}+\frac{\mathfrak{V}_6}{\mathcal{R}_Y}\right)\frac{\partial^2 \phi_X}{\partial X\partial Y}\\&+\left(\frac{\mathfrak{V}_{47}+\mathfrak{V}_{51}+\chi(\mathfrak{V}_{59}+\mathfrak{V}_{63})}{R_X}\right)\frac{\partial^2 \mathcal{V}}{\partial X^2}+\frac{\mathfrak{V}_{22}}{\mathcal{R}_Y}\frac{\partial^2 \mathcal{V}}{\partial Y^2}\\&-\frac{\mathfrak{V}_{41}}{\mathcal{R}_Y}\mathcal{V}+\left(\frac{\mathfrak{V}_{49}+\chi\mathfrak{V}_{61}}{R_X}\right)\frac{\partial^2 \phi_Y}{\partial X^2}+\frac{\mathfrak{V}_{24}}{\mathcal{R}_Y}\frac{\partial^2 \phi_Y}{\partial Y^2}\\&+\frac{\mathfrak{V}_{39}}{\mathcal{R}_Y}\phi_Y+\left(\frac{\mathfrak{V}_{40}+\mathfrak{V}_5+\mathfrak{V}_{23}}{\mathcal{R}_Y}\right)\frac{\partial w}{\partial Y}=0\end{aligned} \tag{12c}$$

$$\begin{aligned}&\delta\phi_2:\left(\frac{\mathfrak{V}_{18}}{\mathcal{R}_Y}+\frac{\mathfrak{V}_{60}-\mathfrak{V}_{64}}{R_X}\right)\frac{\partial^2 \mathcal{U}}{\partial X\partial Y}+\left(\frac{\mathfrak{V}_{62}}{R_X}+\frac{\mathfrak{V}_{20}}{\mathcal{R}_Y}\right)\frac{\partial^2 \phi_X}{\partial X\partial Y}\\&+\left(\frac{\mathfrak{V}_{59}+\mathfrak{V}_{63}}{R_X}\right)\frac{\partial^2 \mathcal{V}}{\partial X^2}+\frac{\mathfrak{V}_{28}}{\mathcal{R}_Y}\frac{\partial^2 \mathcal{V}}{\partial Y^2}+\mathfrak{V}_{41}\mathcal{V}\\&+\left(\frac{\mathfrak{V}_{30}}{\mathcal{R}_Y}+\frac{\mathfrak{V}_{61}}{R_X}\right)\frac{\partial^2 \phi_Y}{\partial X^2}-\mathfrak{V}_{39}\phi_Y\\&+\left(\frac{\mathfrak{V}_{29}+\mathfrak{V}_{19}}{\mathcal{R}_Y}-\mathfrak{V}_{40}\right)\frac{\partial w}{\partial Y}=0\end{aligned} \tag{12d}$$

$$\begin{aligned}&\delta w:-\left(\frac{\mathfrak{V}_{11}}{\mathcal{R}_Y}+\frac{\mathfrak{V}_8+\mathfrak{V}_{37}}{R_X}\right)\frac{\partial \mathcal{U}}{\partial X}+\left(\frac{\mathfrak{V}_{35}-\mathfrak{V}_{10}}{R_X}-\frac{\mathfrak{V}_{13}}{\mathcal{R}_Y}\right)\frac{\partial \phi_X}{\partial X}\\&-\left(\frac{\mathfrak{V}_{33}+\mathfrak{V}_{25}}{\mathcal{R}_Y}+\frac{\mathfrak{V}_{11}}{R_X}\right)\frac{\partial \mathcal{V}}{\partial Y}-\left(\frac{\mathfrak{V}}{R_X}+\frac{\mathfrak{V}_{31}}{\mathcal{R}_Y}+\frac{\mathfrak{V}_{27}}{\mathcal{R}_Y}\right)\frac{\partial \phi_Y}{\partial Y}\\&-\left(\frac{\mathfrak{V}_9+\mathfrak{V}_{12}}{R_X}+\frac{\mathfrak{V}_{12}+\mathfrak{V}_{26}}{\mathcal{R}_Y}\right)w+\frac{\mathfrak{V}_{36}}{R_X}\frac{\partial^2 w}{\partial X^2}\\&+\left(\frac{\mathfrak{V}_{32}-\mathfrak{V}_{34}}{\mathcal{R}_Y}\right)\frac{\partial^2 w}{\partial Y^2}-\frac{\mathfrak{V}_{38}}{R_X}\frac{\partial^2 w}{\partial X^2}\\&-\left(\frac{\mathfrak{V}_{14}}{\mathcal{R}_Y}+\frac{\mathfrak{V}_{14}}{R_X}\right)w-\frac{\mathcal{R}_X^{1T}}{R_X^2}\frac{\partial^2 w}{\partial X^2}-\frac{\mathcal{R}_X^{4T}}{R_Y^2}\frac{\partial^2 w}{\partial Y^2}\\&=-\frac{\mathcal{R}_X^{1T}}{R_X}-\frac{\mathcal{R}_X^{4T}}{\mathcal{R}_Y}+q\left(1+\frac{h}{2R_X}\right)\left(1+\frac{h}{2\mathcal{R}_Y}\right)\end{aligned} \tag{12e}$$

2. Solution

In order to investigate the impact of important parameters of the material and loading on the bending results of the graphene origami doubly curved shell, one can extend an analytical approach using the trigonometric functions for satisfying the simply boundary conditions at the edges. Based on this condition, the solution is assumed using the mentioned functions as follows (Lv *et al*. 2024b, Ma *et al*. 2022, Meng *et al*. 2018, 2019, 2024):

One can arrive at the numerical results of deformation $\{\mathbb{U}, \Phi_X, \mathbb{V}, \Phi_Y, \mathbb{W}\}^T$ with substitution of the solution from Eq. (13) into Eq. (12).

$$\begin{Bmatrix}\mathcal{U}\\ \phi_X\\ \mathcal{V}\\ \phi_Y\\ w\end{Bmatrix}=\begin{Bmatrix}\mathbb{U}cos\frac{m\pi X}{L_X}sin\frac{n\pi Y}{L_Y}\\ \Phi_X cos\frac{m\pi X}{L_X}sin\frac{n\pi Y}{L_Y}\\ \mathbb{V}sin\frac{m\pi X}{L_X}cos\frac{n\pi Y}{L_Y}\\ \Phi_Y sin\frac{m\pi X}{L_X}cos\frac{n\pi Y}{L_Y}\\ \mathbb{W}sin\frac{m\pi X}{L_X}sin\frac{n\pi Y}{L_Y}\end{Bmatrix} \tag{13}$$

One can arrive at the numerical results of deformation $\{\mathbb{U}, \Phi_X, \mathbb{V}, \Phi_Y, \mathbb{W}\}^T$ with substitution of the solution from Eq.13 into Eq.12.

Table 1 Comparison between the present results with the literatura works [60, 61]

R/a	Various sources	h/a=0.01	h/a=0.1	h/a=0.15
1	3D (Bhimaraddi 1993)	100.59	8.71	4.95
	PSD (Bhimaraddi 1993)	99.65	7.48	3.89
	CST (Bhimaraddi 1993)	99.64	7.37	3.70
	Mohammad-Rezaei Bidgoli *et al.* (2022)	91.30	7.90	4.51
	Present	90.88	7.78	4.49
2	3D (Bhimaraddi 1993)	396.45	18.45	7.72
	PSD (Bhimaraddi 1993)	394.37	17.01	6.93
	CST (Bhimaraddi 1993)	394.37	16.48	6.33
	Mohammad-Rezaei Bidgoli *et al.* (2022)	360.67	17.55	7.56
	Present	359.01	17.52	7.52
3	3D (Bhimaraddi 1993)	872.02	22.28	8.09
	PSD (Bhimaraddi 1993)	872.02	22.28	8.09
	CST (Bhimaraddi 1993)	872.00	21.37	7.29
	Mohammad-Rezaei Bidgoli *et al.* (2022)	798.11	22.85	8.64
	Present	796.24	22.82	8.60

Table 2 A variation in unknown displacement $\mathcal{U}, \mathcal{V}, \mathcal{w}$ and rotation ϕ_x, ϕ_y components with changes of thermal load $\mathcal{T}$

$\mathcal{T}$	$\mathcal{w}$	$\mathcal{U}$	$\mathcal{V}$	ϕ_x	ϕ_y
300	0.009209	-0.001496	0.001292	-0.029218	-0.028660
302	0.009089	-0.001477	0.001276	-0.028834	-0.028284
304	0.008970	-0.001458	0.001260	-0.028457	-0.027914
306	0.008853	-0.001440	0.001245	-0.028087	-0.027551
308	0.008738	-0.001422	0.001230	-0.027724	-0.027194
310	0.008626	-0.001405	0.001215	-0.027367	-0.026843
312	0.008515	-0.001388	0.001200	-0.027016	-0.026498
314	0.008406	-0.001371	0.001185	-0.026670	-0.026159
316	0.008299	-0.001354	0.001171	-0.026331	-0.025826
318	0.008194	-0.001338	0.001157	-0.025998	-0.025499
320	0.008091	-0.001321	0.001143	-0.025670	-0.025177
322	0.007989	-0.001305	0.001130	-0.025347	-0.024860
324	0.007889	-0.001290	0.001117	-0.025030	-0.024549
326	0.007791	-0.001274	0.001103	-0.024718	-0.024242
328	0.007694	-0.001259	0.001090	-0.024411	-0.023941
330	0.007598	-0.001244	0.001078	-0.024109	-0.023644
332	0.007505	-0.001230	0.001065	-0.023812	-0.023353
334	0.007413	-0.001215	0.001053	-0.023519	-0.023065
336	0.007322	-0.001201	0.001041	-0.023231	-0.022783
338	0.007232	-0.001187	0.001029	-0.022948	-0.022504
340	0.007144	-0.001173	0.001017	-0.022668	-0.022230
342	0.007058	-0.001160	0.001005	-0.022394	-0.021961
344	0.006972	-0.001146	0.000994	-0.022123	-0.021695
346	0.006888	-0.001133	0.000983	-0.021857	-0.021434
348	0.006806	-0.001120	0.000972	-0.021594	-0.021176
350	0.006724	-0.001107	0.000961	-0.021336	-0.020922
352	0.006644	-0.001095	0.000950	-0.021081	-0.020672
354	0.006565	-0.001082	0.000939	-0.020830	-0.020426
356	0.006487	-0.001070	0.000929	-0.020583	-0.020183
358	0.006410	-0.001058	0.000919	-0.020339	-0.019944
360	0.006334	-0.001046	0.000908	-0.020099	-0.019708

Table 3 A variation in unknown displacement $\mathcal{U}, \mathcal{V}, \mathcal{w}$ and rotation ϕ_x, ϕ_y components with changes of volume fraction content V_G

V_G	$\mathcal{w}$	$\mathcal{U}$	$\mathcal{V}$	ϕ_x	ϕ_y
0	0.005308	-0.001128	0.001037	-0.016891	-0.016458
0.001	0.005427	-0.001136	0.001042	-0.017267	-0.016832
0.002	0.005547	-0.001144	0.001046	-0.017645	-0.017207
0.003	0.005667	-0.001152	0.001051	-0.018024	-0.017584
0.004	0.005788	-0.001160	0.001055	-0.018406	-0.017963
0.005	0.00591	-0.001167	0.001059	-0.018790	-0.018345
0.006	0.006032	-0.001175	0.001063	-0.019176	-0.018728
0.007	0.006155	-0.001183	0.001067	-0.019564	-0.019114
0.008	0.006279	-0.001190	0.001070	-0.019954	-0.019502
0.009	0.006404	-0.001198	0.001074	-0.020348	-0.019893
0.01	0.00653	-0.001205	0.001077	-0.020744	-0.020287
0.011	0.006656	-0.001213	0.001081	-0.021142	-0.020684
0.012	0.006783	-0.001221	0.001084	-0.021544	-0.021083
0.013	0.006912	-0.001228	0.001088	-0.021948	-0.021485
0.014	0.007041	-0.001236	0.001091	-0.022356	-0.021891
0.015	0.007171	-0.001243	0.001094	-0.022767	-0.022300
0.016	0.007303	-0.001251	0.001097	-0.023181	-0.022712
0.017	0.007435	-0.001259	0.001101	-0.023599	-0.023127
0.018	0.007569	-0.001267	0.001104	-0.024020	-0.023546
0.019	0.007704	-0.001274	0.001107	-0.024445	-0.023969
0.02	0.00784	-0.001282	0.001110	-0.024873	-0.024395
0.021	0.007977	-0.001290	0.001113	-0.025306	-0.024825
0.022	0.008115	-0.001298	0.001116	-0.025742	-0.025259
0.023	0.008255	-0.001306	0.001119	-0.026182	-0.025697
0.024	0.008396	-0.001314	0.001122	-0.026627	-0.026140
0.025	0.008538	-0.001322	0.001125	-0.027076	-0.026586
0.026	0.008682	-0.001331	0.001128	-0.027529	-0.027037
0.027	0.008827	-0.001339	0.001131	-0.027986	-0.027492
0.028	0.008974	-0.001347	0.001134	-0.028448	-0.027952
0.029	0.009122	-0.001356	0.001137	-0.028915	-0.028417
0.03	0.009271	-0.001365	0.001140	-0.029387	-0.028886

3. Numerical results and discussion

This sections investigates impact of the material characteristics of the graphene origami on the bending deformation and strain components of the double curved shell reinforced with 3D nanofillers. In order to seek trueness and accuracy of the formulation and results and

Table 4 A variation in unknown displacement $\mathcal{U}, \mathcal{V}, \mathcal{w}$ and rotation ϕ_x, ϕ_y components with changes of foldability parameter H_G

H_G	$\mathcal{w}$	$\mathcal{U}$	$\mathcal{V}$	ϕ_x	ϕ_y
0	0.004161	-0.000859	0.000786	-0.013237	-0.012908
0.02	0.004226	-0.000868	0.000793	-0.013441	-0.013109
0.04	0.004291	-0.000876	0.000800	-0.013647	-0.013311
0.06	0.004356	-0.000885	0.000807	-0.013853	-0.013515
0.08	0.004421	-0.000894	0.000814	-0.014060	-0.013719
0.1	0.004487	-0.000902	0.000821	-0.014269	-0.013924
0.12	0.004553	-0.000911	0.000828	-0.014478	-0.014131
0.14	0.00462	-0.000920	0.000835	-0.014689	-0.014338
0.16	0.004687	-0.000928	0.000842	-0.014900	-0.014546
0.18	0.004754	-0.000937	0.000849	-0.015113	-0.014756
0.2	0.004821	-0.000945	0.000856	-0.015326	-0.014966
0.22	0.004889	-0.000954	0.000863	-0.015541	-0.015178
0.24	0.004957	-0.000962	0.000869	-0.015757	-0.015390
0.26	0.005026	-0.000971	0.000876	-0.015973	-0.015604
0.28	0.005094	-0.000979	0.000883	-0.016191	-0.015819
0.3	0.005164	-0.000988	0.000890	-0.016410	-0.016035
0.32	0.005233	-0.000996	0.000896	-0.016630	-0.016252
0.34	0.005303	-0.001004	0.000903	-0.016852	-0.016470
0.36	0.005373	-0.001013	0.000909	-0.017074	-0.016689
0.38	0.005444	-0.001021	0.000916	-0.017297	-0.016910
0.4	0.005515	-0.001030	0.000923	-0.017522	-0.017132
0.42	0.005586	-0.001038	0.000929	-0.017748	-0.017354
0.44	0.005658	-0.001046	0.000936	-0.017975	-0.017579
0.46	0.00573	-0.001055	0.000942	-0.018203	-0.017804
0.48	0.005803	-0.001063	0.000949	-0.018433	-0.018030
0.5	0.005876	-0.001071	0.000955	-0.018663	-0.018258
0.52	0.005949	-0.001080	0.000961	-0.018895	-0.018487
0.54	0.006023	-0.001088	0.000968	-0.019128	-0.018717
0.56	0.006097	-0.001097	0.000974	-0.019363	-0.018949
0.58	0.006171	-0.001105	0.000980	-0.019598	-0.019181
0.6	0.006246	-0.001113	0.000987	-0.019836	-0.019416

Table 5 thickness-dependent variation in normal strain ε_x with changes of thermal load $\mathcal{T}$

$\mathcal{T}$	z=-0.005	z=-0.0025	z=0	z=+0.0025	z=+0.005
300	0.001522	0.001749	0.001976	0.002203	0.002430
302	0.001410	0.001634	0.001858	0.002082	0.002306
304	0.001299	0.001520	0.001742	0.001963	0.002184
306	0.001190	0.001408	0.001627	0.001845	0.002063
308	0.001081	0.001297	0.001513	0.001728	0.001943
310	0.000975	0.001188	0.001400	0.001613	0.001825
312	0.000869	0.001079	0.001289	0.001499	0.001709
314	0.000764	0.000972	0.001179	0.001386	0.001593
316	0.000661	0.000866	0.001071	0.001275	0.001479
318	0.000558	0.000761	0.000963	0.001165	0.001367
320	0.000457	0.000657	0.000857	0.001056	0.001255
322	0.000357	0.000554	0.000751	0.000948	0.001145
324	0.000258	0.000452	0.000647	0.000842	0.001036
326	0.000159	0.000352	0.000544	0.000736	0.000928
328	0.000062	0.000252	0.000442	0.000632	0.000821
330	-0.000034	0.000153	0.000341	0.000528	0.000715
332	-0.000130	0.000056	0.000241	0.000426	0.000611
334	-0.000224	-0.000041	0.000142	0.000324	0.000507
336	-0.000318	-0.000137	0.000044	0.000224	0.000404
338	-0.000411	-0.000232	-0.000054	0.000125	0.000303
340	-0.000503	-0.000326	-0.000150	0.000026	0.000202
342	-0.000594	-0.000420	-0.000245	-0.000071	0.000102
344	-0.000684	-0.000512	-0.000340	-0.000168	0.000004
346	-0.000774	-0.000604	-0.000434	-0.000264	-0.000094
348	-0.000863	-0.000695	-0.000527	-0.000359	-0.000191
350	-0.000951	-0.000785	-0.000619	-0.000453	-0.000287
352	-0.001038	-0.000874	-0.000710	-0.000546	-0.000383
354	-0.001125	-0.000963	-0.000801	-0.000639	-0.000477
356	-0.001211	-0.001050	-0.000890	-0.000730	-0.000571
358	-0.001296	-0.001138	-0.000979	-0.000821	-0.000664
360	-0.001380	-0.001224	-0.001068	-0.000912	-0.000756

verification of the present study, Table 1 is provided to address.

The material properties of Cu matrix and graphene origami as assumed as:

$E_C = 65.79GPa, \quad E_G = 929.57GPa, \quad \vartheta_C = 0.387,$

$\vartheta_G = 0.22, \ \alpha_C = 16.51 \times 10^{-6} \frac{1}{K^o},$

$\vartheta_G = -3.98 \times 10^{-6} \frac{1}{K^o}, \quad l_G = 83.76 \times 10^{-10} m,$

$t_G = 3.4 \times 10^{-10} m,$

Table 2 lists variation in all displacement $\mathcal{U}, \mathcal{V}, \mathcal{w}$ and rotation components ϕ_x, ϕ_y with changes of thermal loads. One can conclude that the results are decreased with an enhancement in thermal loads.

Tables 3, 4 list variation in all displacement $\mathcal{U}, \mathcal{V}, \mathcal{w}$ and rotation components ϕ_x, ϕ_y with changes of origami content and foldability parameter, respectively. It is deduced that the mentioned components are increased with an enhancement in origami content. Furthermore an enhancement in the all displacement $\mathcal{U}, \mathcal{V}, \mathcal{w}$ and rotation components ϕ_x, ϕ_y is observed with an enhancement in the foldability parameter.

Listed in the Tables 5, 6 and 7 are variation in in-plane strain component ε_x with changes of thermal loads, origami content, and foldability parameter along the thickness direction. A decrease in in-plane strain component ε_x is observed with an enhancement in thermal loads, origami content, and foldability parameter. Regard to the results presented in Table 6, it is concluded that an enhancement in volume fraction of the graphene origami leads to an increase in structural stiffness and consequently a decrease in the strain components.

Table 6 thickness-dependent variation in normal strain ε_x with changes of graphene origami content V_G

V_G	z=-0.005	z=-0.0025	z=0	z=+0.0025	z=+0.005
0	-0.000798	-0.000667	-0.000536	-0.000406	-0.000275
0.001	-0.000750	-0.000616	-0.000482	-0.000348	-0.000215
0.002	-0.000701	-0.000564	-0.000428	-0.000291	-0.000154
0.003	-0.000653	-0.000513	-0.000373	-0.000234	-0.000094
0.004	-0.000604	-0.000462	-0.000319	-0.000176	-0.000034
0.005	-0.000556	-0.000410	-0.000264	-0.000118	0.000027
0.006	-0.000507	-0.000358	-0.000209	-0.000061	0.000088
0.007	-0.000458	-0.000306	-0.000154	-0.000002	0.000149
0.008	-0.000409	-0.000254	-0.000099	0.000056	0.000210
0.009	-0.000359	-0.000201	-0.000043	0.000115	0.000272
0.01	-0.000310	-0.000149	0.000013	0.000174	0.000334
0.011	-0.000260	-0.000095	0.000069	0.000233	0.000397
0.012	-0.000209	-0.000042	0.000125	0.000293	0.000460
0.013	-0.000159	0.000012	0.000183	0.000353	0.000523
0.014	-0.000108	0.000066	0.000240	0.000414	0.000587
0.015	-0.000056	0.000121	0.000298	0.000475	0.000651
0.016	-0.000004	0.000176	0.000356	0.000536	0.000716
0.017	0.000048	0.000232	0.000415	0.000599	0.000782
0.018	0.000101	0.000288	0.000475	0.000661	0.000848
0.019	0.000154	0.000345	0.000535	0.000725	0.000914
0.02	0.000208	0.000402	0.000595	0.000789	0.000982
0.021	0.000263	0.000460	0.000657	0.000853	0.001050
0.022	0.000318	0.000518	0.000718	0.000918	0.001118
0.023	0.000373	0.000577	0.000781	0.000984	0.001188
0.024	0.000429	0.000637	0.000844	0.001051	0.001258
0.025	0.000486	0.000697	0.000908	0.001118	0.001329
0.026	0.000544	0.000758	0.000972	0.001186	0.001400
0.027	0.000602	0.000820	0.001038	0.001255	0.001473
0.028	0.000660	0.000882	0.001103	0.001325	0.001546
0.029	0.000720	0.000945	0.001170	0.001395	0.001620
0.03	0.000780	0.001009	0.001238	0.001466	0.001695

Table 7 thickness-dependent variation in normal strain ε_x with changes of graphene origami foldability H_G

H_G	z=-0.005	z=-0.0025	z=0	z=+0.0025	z=+0.005
0	-0.001675	-0.001572	-0.001469	-0.001367	-0.001264
0.02	-0.001638	-0.001533	-0.001429	-0.001325	-0.001221
0.04	-0.001601	-0.001495	-0.001389	-0.001283	-0.001177
0.06	-0.001564	-0.001456	-0.001349	-0.001241	-0.001134
0.08	-0.001527	-0.001417	-0.001308	-0.001199	-0.001090
0.1	-0.001490	-0.001379	-0.001268	-0.001157	-0.001047
0.12	-0.001453	-0.001340	-0.001228	-0.001116	-0.001004
0.14	-0.001416	-0.001302	-0.001188	-0.001074	-0.000960
0.16	-0.001379	-0.001263	-0.001147	-0.001032	-0.000916
0.18	-0.001342	-0.001224	-0.001107	-0.000990	-0.000873
0.2	-0.001305	-0.001186	-0.001067	-0.000948	-0.000829
0.22	-0.001268	-0.001147	-0.001027	-0.000906	-0.000786
0.24	-0.001231	-0.001109	-0.000986	-0.000864	-0.000742
0.26	-0.001194	-0.001070	-0.000946	-0.000822	-0.000698
0.28	-0.001157	-0.001031	-0.000906	-0.000780	-0.000655
0.3	-0.001120	-0.000993	-0.000865	-0.000738	-0.000611
0.32	-0.001083	-0.000954	-0.000825	-0.000696	-0.000567
0.34	-0.001046	-0.000915	-0.000785	-0.000654	-0.000523
0.36	-0.001009	-0.000877	-0.000744	-0.000612	-0.000479
0.38	-0.000972	-0.000838	-0.000704	-0.000569	-0.000435
0.4	-0.000935	-0.000799	-0.000663	-0.000527	-0.000391
0.42	-0.000898	-0.000760	-0.000622	-0.000485	-0.000347
0.44	-0.000861	-0.000721	-0.000582	-0.000442	-0.000303
0.46	-0.000824	-0.000682	-0.000541	-0.000400	-0.000259
0.48	-0.000787	-0.000643	-0.000500	-0.000357	-0.000214
0.5	-0.000749	-0.000604	-0.000459	-0.000314	-0.000170
0.52	-0.000712	-0.000565	-0.000418	-0.000272	-0.000125
0.54	-0.000675	-0.000526	-0.000377	-0.000229	-0.000081
0.56	-0.000637	-0.000487	-0.000336	-0.000186	-0.000036
0.58	-0.000600	-0.000447	-0.000295	-0.000143	0.000009
0.6	-0.000562	-0.000408	-0.000254	-0.000100	0.000054

Table 8 Thickness-dependent variation in normal strain ε_y with changes of thermal load $\mathcal{T}$

$\mathcal{T}$	z=-0.005	z=-0.0025	z=0	z=+0.0025	z=+0.005
300	-0.007236	-0.007009	-0.006782	-0.006555	-0.006328
302	-0.007239	-0.007014	-0.006790	-0.006566	-0.006342
304	-0.007242	-0.007020	-0.006799	-0.006578	-0.006357
306	-0.007246	-0.007027	-0.006808	-0.006590	-0.006372
308	-0.007250	-0.007034	-0.006818	-0.006603	-0.006388
310	-0.007254	-0.007041	-0.006829	-0.006616	-0.006404
312	-0.007260	-0.007049	-0.006839	-0.006629	-0.006420
314	-0.007266	-0.007058	-0.006851	-0.006643	-0.006436
316	-0.007272	-0.007067	-0.006862	-0.006658	-0.006453
318	-0.007279	-0.007076	-0.006874	-0.006672	-0.006470
320	-0.007286	-0.007086	-0.006887	-0.006687	-0.006488
322	-0.007294	-0.007097	-0.006900	-0.006703	-0.006506
324	-0.007302	-0.007107	-0.006913	-0.006718	-0.006524
326	-0.007311	-0.007119	-0.006926	-0.006734	-0.006542
328	-0.007320	-0.007130	-0.006940	-0.006751	-0.006561
330	-0.007330	-0.007142	-0.006955	-0.006767	-0.006580
332	-0.007340	-0.007155	-0.006969	-0.006784	-0.006600
334	-0.007350	-0.007167	-0.006984	-0.006802	-0.006619
336	-0.007361	-0.007180	-0.007000	-0.006819	-0.006639
338	-0.007373	-0.007194	-0.007015	-0.006837	-0.006659
340	-0.007384	-0.007208	-0.007031	-0.006855	-0.006679
342	-0.007396	-0.007222	-0.007048	-0.006874	-0.006700
344	-0.007409	-0.007237	-0.007064	-0.006893	-0.006721
346	-0.007422	-0.007251	-0.007081	-0.006912	-0.006742
348	-0.007435	-0.007267	-0.007099	-0.006931	-0.006763

350	-0.007448	-0.007282	-0.007116	-0.006951	-0.006785
352	-0.007462	-0.007298	-0.007134	-0.006970	-0.006807
354	-0.007476	-0.007314	-0.007152	-0.006990	-0.006829
356	-0.007491	-0.007331	-0.007171	-0.007011	-0.006851
358	-0.007506	-0.007348	-0.007189	-0.007031	-0.006874
360	-0.007521	-0.007365	-0.007208	-0.007052	-0.006896

Table 9 Thickness-dependent variation in normal strain ε_y with changes of origami content V_G

V_G	z=-0.005	z=-0.0025	z=0	z=+0.0025	z=+0.005
0	-0.007601	-0.007470	-0.007339	-0.007208	-0.007078
0.001	-0.007592	-0.007458	-0.007325	-0.007191	-0.007057
0.002	-0.007583	-0.007446	-0.007309	-0.007172	-0.007036
0.003	-0.007572	-0.007432	-0.007293	-0.007153	-0.007013
0.004	-0.007561	-0.007418	-0.007276	-0.007133	-0.006990
0.005	-0.007550	-0.007404	-0.007258	-0.007112	-0.006967
0.006	-0.007537	-0.007388	-0.007239	-0.007091	-0.006942
0.007	-0.007524	-0.007372	-0.007220	-0.007069	-0.006917
0.008	-0.007511	-0.007356	-0.007201	-0.007046	-0.006891
0.009	-0.007496	-0.007338	-0.007180	-0.007022	-0.006865
0.01	-0.007482	-0.007320	-0.007159	-0.006998	-0.006838
0.011	-0.007466	-0.007302	-0.007138	-0.006974	-0.006810
0.012	-0.007451	-0.007283	-0.007116	-0.006949	-0.006781
0.013	-0.007434	-0.007264	-0.007093	-0.006923	-0.006752
0.014	-0.007417	-0.007244	-0.007070	-0.006896	-0.006723
0.015	-0.007400	-0.007223	-0.007046	-0.006869	-0.006693
0.016	-0.007382	-0.007202	-0.007022	-0.006842	-0.006662
0.017	-0.007364	-0.007180	-0.006997	-0.006814	-0.006631
0.018	-0.007345	-0.007158	-0.006972	-0.006785	-0.006599
0.019	-0.007326	-0.007136	-0.006946	-0.006756	-0.006566
0.02	-0.007307	-0.007113	-0.006919	-0.006726	-0.006533
0.021	-0.007287	-0.007089	-0.006893	-0.006696	-0.006500
0.022	-0.007266	-0.007066	-0.006865	-0.006665	-0.006465
0.023	-0.007245	-0.007041	-0.006838	-0.006634	-0.006431
0.024	-0.007224	-0.007016	-0.006809	-0.006602	-0.006396
0.025	-0.007202	-0.006991	-0.006780	-0.006570	-0.006360
0.026	-0.007180	-0.006965	-0.006751	-0.006537	-0.006323
0.027	-0.007157	-0.006939	-0.006721	-0.006504	-0.006286
0.028	-0.007134	-0.006913	-0.006691	-0.006470	-0.006249
0.029	-0.007111	-0.006886	-0.006661	-0.006436	-0.006211
0.03	-0.007087	-0.006858	-0.006629	-0.006401	-0.006172

Listed in the Tables 8, 9 and 10 are variation in in-plane strain component ε_y with changes of thermal loads, origami content, and foldability parameter along the thickness direction. An increase in in-plane strain component ε_y is observed with an enhancement in the thermal loads and foldability parameter of the graphene origami. Furthermore, it is observed that the in-plane strain component ε_y is decreased with an enhancement in the

Table 10 Thickness-dependent variation in normal strain ε_y with changes of foldability parameter H_G

H_G	z=-0.005	z=-0.0025	z=0	z=+0.0025	z=+0.005
0	-0.006842	-0.006739	-0.006636	-0.006534	-0.006431
0.02	-0.006855	-0.006750	-0.006646	-0.006542	-0.006438
0.04	-0.006867	-0.006761	-0.006656	-0.006550	-0.006444
0.06	-0.006880	-0.006772	-0.006665	-0.006558	-0.006450
0.08	-0.006892	-0.006783	-0.006674	-0.006565	-0.006456
0.1	-0.006905	-0.006794	-0.006683	-0.006572	-0.006462
0.12	-0.006917	-0.006804	-0.006692	-0.006580	-0.006467
0.14	-0.006928	-0.006814	-0.006700	-0.006586	-0.006473
0.16	-0.006940	-0.006824	-0.006709	-0.006593	-0.006478
0.18	-0.006952	-0.006834	-0.006717	-0.006600	-0.006483
0.2	-0.006963	-0.006844	-0.006725	-0.006606	-0.006487
0.22	-0.006974	-0.006853	-0.006733	-0.006612	-0.006492
0.24	-0.006985	-0.006863	-0.006741	-0.006618	-0.006496
0.26	-0.006996	-0.006872	-0.006748	-0.006624	-0.006500
0.28	-0.007007	-0.006881	-0.006755	-0.006630	-0.006504
0.3	-0.007017	-0.006890	-0.006763	-0.006635	-0.006508
0.32	-0.007028	-0.006899	-0.006770	-0.006641	-0.006512
0.34	-0.007038	-0.006907	-0.006776	-0.006646	-0.006515
0.36	-0.007048	-0.006916	-0.006783	-0.006651	-0.006518
0.38	-0.007058	-0.006924	-0.006790	-0.006655	-0.006521
0.4	-0.007068	-0.006932	-0.006796	-0.006660	-0.006524
0.42	-0.007078	-0.006940	-0.006802	-0.006664	-0.006527
0.44	-0.007088	-0.006948	-0.006808	-0.006669	-0.006529
0.46	-0.007097	-0.006955	-0.006814	-0.006673	-0.006532
0.48	-0.007106	-0.006963	-0.006820	-0.006677	-0.006534
0.5	-0.007115	-0.006970	-0.006825	-0.006681	-0.006536

Table 11 Thickness-dependent variation in normal strain γ_{xy} with changes of thermal load $\mathcal{T}$

$\mathcal{T}$	z=-0.005	z=-0.0025	z=0	z=+0.0025	z=+0.005
300	0.000270	-0.000185	-0.000640	-0.001094	-0.001547
302	0.000266	-0.000183	-0.000631	-0.001079	-0.001527
304	0.000263	-0.000180	-0.000623	-0.001065	-0.001506
306	0.000260	-0.000177	-0.000614	-0.001051	-0.001487
308	0.000257	-0.000175	-0.000606	-0.001037	-0.001467
310	0.000254	-0.000172	-0.000598	-0.001023	-0.001448
312	0.000251	-0.000169	-0.000590	-0.001009	-0.001429
314	0.000248	-0.000167	-0.000582	-0.000996	-0.001410
316	0.000245	-0.000165	-0.000574	-0.000983	-0.001392
318	0.000243	-0.000162	-0.000567	-0.000971	-0.001374
320	0.000240	-0.000160	-0.000559	-0.000958	-0.001356
322	0.000237	-0.000158	-0.000552	-0.000946	-0.001339
324	0.000234	-0.000155	-0.000545	-0.000934	-0.001322
326	0.000232	-0.000153	-0.000538	-0.000922	-0.001305
328	0.000229	-0.000151	-0.000531	-0.000910	-0.001289
330	0.000227	-0.000149	-0.000524	-0.000898	-0.001273

332	0.000224	-0.000147	-0.000517	-0.000887	-0.001257
334	0.000222	-0.000145	-0.000510	-0.000876	-0.001241
336	0.000219	-0.000143	-0.000504	-0.000865	-0.001225
338	0.000217	-0.000141	-0.000497	-0.000854	-0.001210
340	0.000214	-0.000139	-0.000491	-0.000843	-0.001195
342	0.000212	-0.000137	-0.000485	-0.000833	-0.001180
344	0.000210	-0.000135	-0.000479	-0.000823	-0.001166
346	0.000207	-0.000133	-0.000473	-0.000812	-0.001152
348	0.000205	-0.000131	-0.000467	-0.000802	-0.001138
350	0.000203	-0.000129	-0.000461	-0.000792	-0.001124

Table 12 Thickness-dependent variation in normal strain γ_{xy} with changes of origami content V_G

V_G	z=-0.005	z=-0.0025	z=0	z=+0.0025	z=+0.005
0	0.000238	-0.000025	-0.000286	-0.000548	-0.000809
0.001	0.000239	-0.000029	-0.000297	-0.000565	-0.000832
0.002	0.000240	-0.000034	-0.000308	-0.000581	-0.000854
0.003	0.000241	-0.000039	-0.000319	-0.000598	-0.000877
0.004	0.000241	-0.000045	-0.000330	-0.000615	-0.000901
0.005	0.000242	-0.000050	-0.000342	-0.000633	-0.000924
0.006	0.000242	-0.000056	-0.000353	-0.000651	-0.000948
0.007	0.000243	-0.000061	-0.000365	-0.000669	-0.000972
0.008	0.000243	-0.000067	-0.000377	-0.000687	-0.000996
0.009	0.000243	-0.000074	-0.000390	-0.000705	-0.001021
0.01	0.000243	-0.000080	-0.000402	-0.000724	-0.001046
0.011	0.000242	-0.000086	-0.000415	-0.000743	-0.001071
0.012	0.000242	-0.000093	-0.000428	-0.000762	-0.001096
0.013	0.000241	-0.000100	-0.000441	-0.000782	-0.001122
0.014	0.000241	-0.000107	-0.000455	-0.000802	-0.001149
0.015	0.000240	-0.000115	-0.000468	-0.000822	-0.001175
0.016	0.000239	-0.000122	-0.000482	-0.000842	-0.001202
0.017	0.000237	-0.000130	-0.000497	-0.000863	-0.001229
0.018	0.000236	-0.000138	-0.000511	-0.000884	-0.001257
0.019	0.000235	-0.000146	-0.000526	-0.000906	-0.001285
0.02	0.000233	-0.000154	-0.000541	-0.000928	-0.001314
0.021	0.000231	-0.000163	-0.000556	-0.000950	-0.001342
0.022	0.000229	-0.000171	-0.000572	-0.000972	-0.001372
0.023	0.000227	-0.000180	-0.000588	-0.000995	-0.001401
0.024	0.000225	-0.000190	-0.000604	-0.001018	-0.001431
0.025	0.000223	-0.000199	-0.000620	-0.001041	-0.001462

Table 13 Thickness-dependent variation in normal strain γ_{xy} with changes of foldability parameter H_G

H_G	z=-0.005	z=-0.0025	z=0	z=+0.0025	z=+0.005
0	0.000180	-0.000025	-0.000231	-0.000436	-0.000641
0.02	0.000182	-0.000027	-0.000236	-0.000444	-0.000652
0.04	0.000183	-0.000029	-0.000240	-0.000452	-0.000663
0.06	0.000185	-0.000030	-0.000245	-0.000460	-0.000674
0.08	0.000186	-0.000032	-0.000250	-0.000468	-0.000686
0.1	0.000188	-0.000034	-0.000255	-0.000476	-0.000697
0.12	0.000190	-0.000035	-0.000260	-0.000484	-0.000709
0.14	0.000191	-0.000037	-0.000265	-0.000493	-0.000720
0.16	0.000193	-0.000039	-0.000270	-0.000501	-0.000732
0.18	0.000194	-0.000041	-0.000275	-0.000510	-0.000744
0.2	0.000195	-0.000043	-0.000281	-0.000518	-0.000756
0.22	0.000197	-0.000045	-0.000286	-0.000527	-0.000768
0.24	0.000198	-0.000047	-0.000291	-0.000536	-0.000780
0.26	0.000200	-0.000049	-0.000297	-0.000544	-0.000792
0.28	0.000201	-0.000051	-0.000302	-0.000553	-0.000804
0.3	0.000202	-0.000053	-0.000308	-0.000562	-0.000816
0.32	0.000204	-0.000055	-0.000313	-0.000571	-0.000829
0.34	0.000205	-0.000057	-0.000319	-0.000580	-0.000841
0.36	0.000206	-0.000059	-0.000325	-0.000589	-0.000854
0.38	0.000207	-0.000062	-0.000330	-0.000599	-0.000867
0.4	0.000208	-0.000064	-0.000336	-0.000608	-0.000880
0.42	0.000210	-0.000066	-0.000342	-0.000617	-0.000892
0.44	0.000211	-0.000069	-0.000348	-0.000627	-0.000905
0.46	0.000212	-0.000071	-0.000354	-0.000636	-0.000919
0.48	0.000213	-0.000074	-0.000360	-0.000646	-0.000932
0.5	0.000214	-0.000076	-0.000366	-0.000656	-0.000945

Table 14 Thickness-dependent variation in normal strain γ_{xz} with changes of thermal load $\mathcal{T}$

$\mathcal{T}$	z=-0.005	z=-0.0025	z=0	z=+0.0025	z=+0.005
300	0.0000428	0.0000283	0.0000138	-0.0000007	-0.0000151
302	0.0000422	0.0000279	0.0000136	-0.0000007	-0.0000149
304	0.0000417	0.0000275	0.0000134	-0.0000006	-0.0000147
306	0.0000411	0.0000272	0.0000133	-0.0000006	-0.0000145
308	0.0000406	0.0000268	0.0000131	-0.0000006	-0.0000143
310	0.0000401	0.0000265	0.0000129	-0.0000006	-0.0000141
312	0.0000396	0.0000262	0.0000128	-0.0000006	-0.0000139
314	0.0000391	0.0000258	0.0000126	-0.0000006	-0.0000137
316	0.0000386	0.0000255	0.0000125	-0.0000006	-0.0000136
318	0.0000381	0.0000252	0.0000123	-0.0000005	-0.0000134
320	0.0000376	0.0000249	0.0000122	-0.0000005	-0.0000132
322	0.0000372	0.0000246	0.0000120	-0.0000005	-0.0000130
324	0.0000367	0.0000243	0.0000119	-0.0000005	-0.0000129
326	0.0000362	0.0000240	0.0000117	-0.0000005	-0.0000127
328	0.0000358	0.0000237	0.0000116	-0.0000005	-0.0000125
330	0.0000354	0.0000234	0.0000115	-0.0000005	-0.0000124
332	0.0000349	0.0000231	0.0000113	-0.0000005	-0.0000122
334	0.0000345	0.0000228	0.0000112	-0.0000004	-0.0000121
336	0.0000341	0.0000226	0.0000111	-0.0000004	-0.0000119
338	0.0000337	0.0000223	0.0000109	-0.0000004	-0.0000118
340	0.0000333	0.0000220	0.0000108	-0.0000004	-0.0000116

Table 15 Thickness-dependent variation in normal strain γ_{XZ} with changes of origami content V_G

V_G	z=-0.005	z=-0.0025	z=0	z=+0.0025	z=+0.005
0	0.0000269	0.0000186	0.0000102	0.0000019	-0.0000064
0.001	0.0000274	0.0000188	0.0000103	0.0000018	-0.0000067
0.002	0.0000278	0.0000191	0.0000104	0.0000017	-0.0000070
0.003	0.0000283	0.0000194	0.0000105	0.0000016	-0.0000073
0.004	0.0000288	0.0000197	0.0000106	0.0000015	-0.0000076
0.005	0.0000292	0.0000199	0.0000106	0.0000014	-0.0000079
0.006	0.0000297	0.0000202	0.0000107	0.0000012	-0.0000082
0.007	0.0000302	0.0000205	0.0000108	0.0000011	-0.0000085
0.008	0.0000306	0.0000207	0.0000109	0.0000010	-0.0000088
0.009	0.0000311	0.0000210	0.0000110	0.0000009	-0.0000091
0.01	0.0000316	0.0000213	0.0000110	0.0000008	-0.0000095
0.011	0.0000320	0.0000216	0.0000111	0.0000007	-0.0000098
0.012	0.0000325	0.0000218	0.0000112	0.0000005	-0.0000101
0.013	0.0000330	0.0000221	0.0000113	0.0000004	-0.0000104
0.014	0.0000335	0.0000224	0.0000113	0.0000003	-0.0000108
0.015	0.0000340	0.0000227	0.0000114	0.0000002	-0.0000111
0.016	0.0000345	0.0000230	0.0000115	0.0000000	-0.0000114
0.017	0.0000350	0.0000233	0.0000116	-0.0000001	-0.0000118
0.018	0.0000355	0.0000236	0.0000117	-0.0000002	-0.0000121
0.019	0.0000360	0.0000238	0.0000117	-0.0000004	-0.0000124
0.02	0.0000365	0.0000241	0.0000118	-0.0000005	-0.0000128
0.021	0.0000370	0.0000244	0.0000119	-0.0000006	-0.0000131
0.022	0.0000375	0.0000247	0.0000120	-0.0000008	-0.0000135
0.023	0.0000380	0.0000250	0.0000121	-0.0000009	-0.0000138
0.024	0.0000385	0.0000253	0.0000121	-0.0000010	-0.0000142
0.025	0.0000391	0.0000256	0.0000122	-0.0000012	-0.0000146

Table 16 Thickness-dependent variation in normal strain γ_{XZ} with changes of origami foldability H_G

H_G	z=-0.005	z=-0.0025	z=0	z=+0.0025	z=+0.005
0	0.0000209	0.0000143	0.0000078	0.0000013	-0.0000053
0.02	0.0000212	0.0000145	0.0000079	0.0000013	-0.0000054
0.04	0.0000215	0.0000147	0.0000080	0.0000012	-0.0000055
0.06	0.0000217	0.0000149	0.0000080	0.0000012	-0.0000056
0.08	0.0000220	0.0000151	0.0000081	0.0000012	-0.0000057
0.1	0.0000223	0.0000153	0.0000082	0.0000012	-0.0000059
0.12	0.0000226	0.0000154	0.0000083	0.0000011	-0.0000060
0.14	0.0000229	0.0000156	0.0000084	0.0000011	-0.0000061
0.16	0.0000232	0.0000158	0.0000085	0.0000011	-0.0000063
0.18	0.0000235	0.0000160	0.0000085	0.0000011	-0.0000064
0.2	0.0000238	0.0000162	0.0000086	0.0000010	-0.0000065
0.22	0.0000241	0.0000164	0.0000087	0.0000010	-0.0000066
0.24	0.0000244	0.0000166	0.0000088	0.0000010	-0.0000068
0.26	0.0000247	0.0000168	0.0000089	0.0000010	-0.0000069
0.28	0.0000250	0.0000169	0.0000089	0.0000009	-0.0000071
0.3	0.0000253	0.0000171	0.0000090	0.0000009	-0.0000072
0.32	0.0000256	0.0000173	0.0000091	0.0000009	-0.0000073
0.34	0.0000259	0.0000175	0.0000092	0.0000008	-0.0000075
0.36	0.0000262	0.0000177	0.0000093	0.0000008	-0.0000076
0.38	0.0000265	0.0000179	0.0000093	0.0000008	-0.0000078
0.4	0.0000268	0.0000181	0.0000094	0.0000008	-0.0000079
0.42	0.0000271	0.0000183	0.0000095	0.0000007	-0.0000080
0.44	0.0000274	0.0000185	0.0000096	0.0000007	-0.0000082
0.46	0.0000277	0.0000187	0.0000097	0.0000007	-0.0000083
0.48	0.0000280	0.0000189	0.0000097	0.0000006	-0.0000085
0.5	0.0000283	0.0000190	0.0000098	0.0000006	-0.0000086

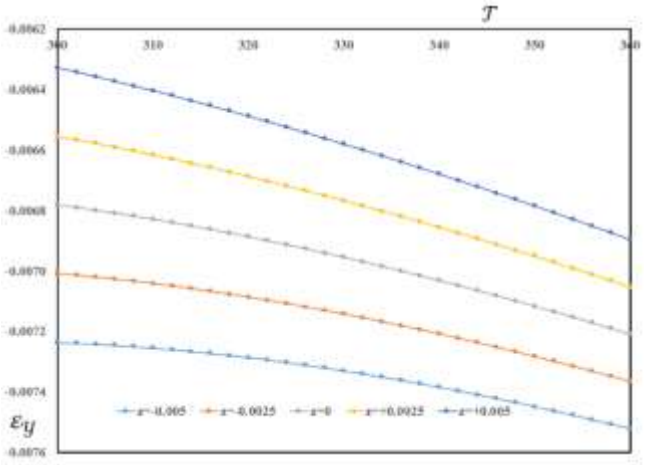

Fig. 1 is variation in strain component ε_y with changes of thermal load $\mathcal{T}$ at various radial coordinates

origami content. One can conclude that an increase in thermal loads leads to an increase in the strain components because of excessive deformation.

Listed in the Tables 11-13 are variation in in-plane strain component γ_{XY} with changes of thermal loads, origami content, and foldability parameter along the thickness direction. An increase in in-plane shear strain component γ_{XY} is observed with an enhancement in the origami content and foldability parameter of the graphene origami. In addition, a decrease in in-plane shear strain component is observed with an enhancement in thermal loads.

Regard to the results of Table 13, it is deduced that an enhancement in the foldability parameter yields a softer nanocomposite material that reflects more strain values.

Listed in the Tables 14-16 are variation in in-plane strain component γ_{XZ} with changes of thermal loads, origami content, and foldability parameter along the thickness direction. An increase in in-plane shear strain component γ_{XZ} is observed with an enhancement in the origami content and foldability parameter of the graphene origami. In addition, a decrease in in-plane shear strain component is observed with an enhancement in origami content.

In order to enhance the numerical results, some graphical results are provided. Shown in Fig. 1 is variation in strain component ε_y with changes of thermal load $\mathcal{T}$ at

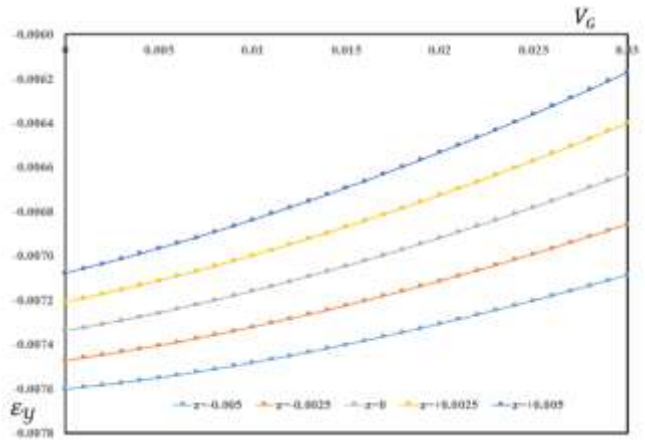

Fig. 2 is variation in strain component ε_y with changes of origami content V_G at various radial coordinates

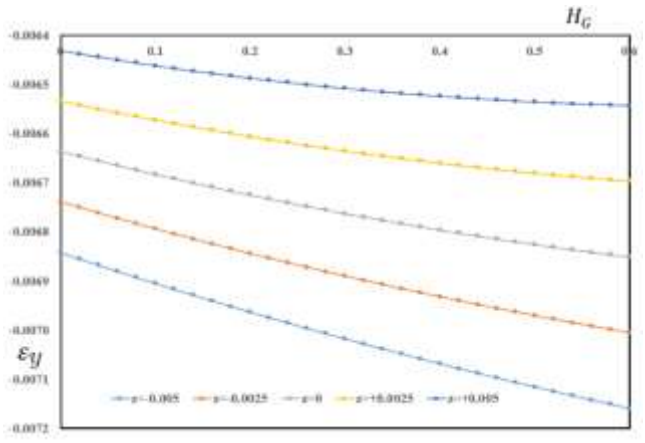

Fig. 3 is variation in strain component ε_y with changes of origami foldability H_G at various radial coordinates

various radial coordinates. The results show an increase in strain components with an enhancement in the thermal loads.

Shown in Figs. 2 and 3 is variation in strain component ε_y with changes of origami content V_G at various radial coordinates, respectively. A decrease in strain is observed with an enhancement in volume fraction of graphene origami. Regard to Fig. 3, an increase in strain is observed with an enhancement in foldability parameter because of decrease in stiffness.

4. Conclusions

In this research work, an analytical study on the deformable analysis of a nanofolded nanocomposite reinforced doubly curved shell is presented using a shear deformable model and a micromechanical model highlights overall material properties. The energy-based formulation was developed to derive the governing equations in terms of primary unknown displacements and rotation components. The solution was extended using an analytical method using the trigonometric functions in order to satisfy boundary conditions. To obtain the overall material characteristics of the copper matrix based nanocomposite structure reinforced with graphene origami, Halpin-Tsai micromechanical model for capturing the impact of material composition is used. The main results of this analysis are classified as follows:
Variation of deformation and strain components with changes of foldability parameter as a significant parameter show an increase in shear strain components because of a decrease in structural stiffness of the constituent materials.
Variation in in-plane normal strain components with changes of the volume fraction of graphene origami as the important affecting parameter show a decrease in the mentioned strain component with an enhancement in origami content.

An increase in in-plane strain component is observed with an enhancement in thermal load because of a decrease in structural stiffness of the constituent material.

Acknowledgements

This work is supported by Natural Science Foundation of Fujian Province, China (2022J02050) and Special Fund granted by Minjiang University (MJY22031), Research Project of Fashu Foundation (MFK24002) and Horizontal Scientific Research Project.

References

Ansari, R. Hassani, R. Gholami, R. Rouhi, H. (2020), "Nonlinear bending analysis of arbitrary-shaped porous nanocomposite plates using a novel numerical approach", *Int. J. Non-Linear Mech.*, **126**, 103556. https://doi.org/10.1016/j.ijnonlinmec.2020.103556

Arefi, M., Rahimi, G.H. (2010), "Thermo elastic analysis of a functionally graded cylinder under internal pressure using first order shear deformation theory", *Sci. Res. Essays*., **5**(12), 1442-1454. https://doi.org/10.5897/SRE.9000953

Arefi, M. Rahimi, G.H. (2011), "Non linear analysis of a functionally graded square plate with two smart layers as sensor and actuator under normal pressure", *Smart. Struct. Syst*., **8**(5), 433-447. https://doi.org/10.12989/sss.2011.8.5.433

Arefi, M. Rahimi, G.H. (2012a), "The effect of nonhomogeneity and end supports on the thermo elastic behavior of a clamped-clamped FG cylinder under mechanical and thermal loads", *Int. J. Pres.Ves. Piping*, **96-97**, 30-37. https://doi.org/10.1016/j.ijpvp.2012.05.009

Arefi, M. Rahimi, G.H. (2012b), "Three-dimensional multi-field equations of a functionally graded piezoelectric thick shell with variable thickness, curvature and arbitrary nonhomogeneity", *Acta. Mech*., **223**, 63-79. https://doi.org/10.1007/s00707-011-0536-5

Arefi, M., Rahimi, G.H. (2012c), "Studying the nonlinear behavior of the functionally graded annular plates with piezoelectric layers as a sensor and actuator under normal pressure", *Smart. Struct. Syst*., **9**(2), 127-143. https://doi.org/10.12989/sss.2012.9.2.127.

Arefi, M., Rahimi, G.H., Khoshgoftar, M.J. (2012), "Exact solution of a thick walled functionally graded piezoelectric cylinder under mechanical, thermal and electrical loads in the magnetic field", *Smart. Struct. Syst*., **9**(5), 427-439. https://doi.org/10.12989/sss.2012.9.5.427

Arefi, M., Allam, M.N.M., (2015), "Nonlinear Responses of an Arbitrary FGP Circular Plate Resting on Foundation", *Smart. Struct. Syst*., **16**(1), 81-100. https://doi.org/10.12989/sss.2015.16.1.081

Arefi, M., Faegh, R.K. Loghman, A. (2016), "The effect of axially variable thermal and mechanical loads on the 2D thermoelastic response of FG cylindrical shell". *J. Therm. Stresses*., **39**, 12, 1539-1559. https://doi.org/10.1080/01495739.2016.1217178.

Arefi, M., Mohammad-Rezaei Bidgoli, E., Zenkour, A.M. (2019), "Free vibration analysis of a sandwich nano-plate including FG core and piezoelectric face-sheets by considering neutral surface", *Mech. Adv. Mater. Struct.*, **26**(9), 741-752. https://doi.org/10.1080/15376494.2018.1455939

Arefi, M., Mohammad-Rezaei Bidgoli, E., Civalek, O. (2020), "Bending response of FG composite doubly curved nanoshells with thickness stretching via higher-order sinusoidal shear theory", *Mech. Based. Design. Struct. Mach.*, **50**(7), 2350-2378. https://doi.org/10.1080/15397734.2020.1777157

Arefi, M., Moghaddam, S.K., Bidgoli, E.M.R., Kiani, M., Civalek, O. (2021), "Analysis of graphene nanoplatelet reinforced cylindrical shell subjected to thermo-mechanical loads", *Compos. Struct.* **255**(1), 112924. https://doi.org/10.1016/j.compstruct.2020.112924.

Arefi, M., Kiani, M. (2020), "Magneto-electro-mechanical bending analysis of three-layered exponentially graded microplate with piezomagnetic face-sheets resting on Pasternak's foundation via MCST", *Mech. Adv. Mater. Struct.*, **27**(5), 383-395 https://doi.org/10.1080/15376494.2018.1473538

Arefi, M., Mohammad-Rezaei Bidgoli, E. (2019) "Electro-elastic displacement and stress analysis of the piezoelectric doubly curved shells resting on Winkler's foundation subjected to applied voltage", *Mech. Adv. Mater. Struct.*, **26**(23), 1981-1994. https://doi.org/10.1080/15376494.2018.1455937.

Arefi, M. (2020), "Size-dependent electro-elastic analysis of a three-layered piezoelectric doubly curved nano shell", *Mech. Adv. Mater. Struct.* **27**(23), 1945-1965. https://doi.org/ 10.1080/15376494.2018.1533605

Arefi, M. (2018), "Nonlocal free vibration analysis of a doubly curved piezoelectric nano shell", *Steel. Compos. Struct.*, **27**(4), 479-493. https://doi.org/10.12989/scs.2018.27.4.479

Arefi, M. (2016), "Analysis of wave in a functionally graded magneto-electro-elastic nano-rod using nonlocal elasticity model subjected to electric and magnetic potentials", *Acta. Mech.*, **227**, 2529-2542. https://doi.org/10.1007/s00707-016-1584-7

Arefi, M., Zenkour, A.M. (2016a), "Free vibration, wave propagation and tension analyses of a sandwich micro/nano rod subjected to electric potential using strain gradient theory" *Mater. Res. Exp.*, **3**(11), 115704. https://doi.org/10.1088/2053-1591/3/11/115704

Arefi, M., Zenkour, A.M. (2016a), "Employing sinusoidal shear deformation plate theory for transient analysis of three layers sandwich nanoplate integrated with piezo-magnetic face-sheets", *Smart. Mater. Struct.*, **25**(11). 115040. https://doi.org/10.1088/0964-1726/25/11/115040

Arefi, M., Zenkour, A.M. (2017a), "Employing the coupled stress components and surface elasticity for nonlocal solution of wave propagation of a functionally graded piezoelectric Love nanorod model", *J. Intel. Mater. Syst. Struct.*, **28**(17), 2403-2413. https://doi.org/10.1177/1045389X17689930

Arefi, M., Zenkour, A.M. (2017b), "Transient sinusoidal shear deformation formulation of a size-dependent three-layer piezo-magnetic curved nanobeam". *Acta. Mech.* **228**, 3657-3674. https://doi.org/10.1007/s00707-017-1892-6

Arefi, M., Zenkour, A.M. (2017c), "Thermo-electro-magneto-mechanical bending behavior of size-dependent sandwich piezomagnetic nanoplates", *Mech. Res. Com.*, **84**, 27-42. https://doi.org/10.1016/j.mechrescom.2017.06.002

Arefi, M., Zenkour, A.M. (2018a), "Size-dependent electro-elastic analysis of a sandwich microbeam based on higher-order sinusoidal shear deformation theory and strain gradient theory", *J. Intel. Mater. Syst. Struct.*, **29**(7), 1394-1406. https://doi.org/10.1177/1045389X17733333

Arefi, M., Zenkour, A.M (2018b), "Free vibration analysis of a three-layered microbeam based on strain gradient theory and three-unknown shear and normal deformation theory", *Steel. Compos. Struct.* **26**(4), 421-437. https://doi.org/10.12989/scs.2018.26.4.421

Arefi, M., Zenkour, A.M. (2019a), "Influence of magneto-electric environments on size-dependent bending results of three-layer piezomagnetic curved nanobeam based on sinusoidal shear deformation theory". *J. Sandw. Struct. Mater.*, **21**(8), 2751-2778. https://doi.org/10.1177/1099636217723186

Arefi, M., Zenkour, A.M. (2019b), "Influence of micro-length-scale parameters and inhomogeneities on the bending, free vibration and wave propagation analyses of a FG Timoshenko's sandwich piezoelectric microbeam", *J. Sandw. Struct. Mater.*, **21**(4), 1243-1270. https://doi.org/10.1177/1099636217714181.

Bai, B., Xu, T., Nie, Q., Li, P. (2020), "Temperature-driven migration of heavy metal Pb2+ along with moisture movement in unsaturated soils". *Int. J. Heat. Mass. Transf.*, **153**, 119573. https://doi.org/10.1016/j.ijheatmasstransfer.2020.119573

Bai, B., Bai, F., Li, X., Nie, Q., Jia, X. (2022), "The remediation efficiency of heavy metal pollutants in water by industrial red mud particle waste". *Env. Tech. Innov.*, **28**, 102944. https://doi.org/10.1016/j.eti.2022.102944

Bai, B., Bai, F., Nie, Q., Jia, X. (2023), "A high-strength red mud-fly ash geopolymer and the implications of curing temperature". *Powd. Tech.*, **416**, 118242. https://doi.org/10.1016/j.powtec.2023.118242

Bai, B., Chen, J., Bai, F., Nie, Q., Jia, X. (2024), "Corrosion effect of acid/alkali on cementitious red mud-fly ash materials containing heavy metal residues". *Env. Tech. Innov.*, **33**, 103485. https://doi.org/10.1016/j.eti.2023.103485

Bai, B., Chen, J., Zhang, B., Chen, L., Zong, Y. (2024), "The solidification of heavy metal Pb2+-contaminated soil by enzyme-induced calcium carbonate precipitation combined with biochar", *Biochem. Eng. J.*, **212**, 109496. https://doi.org/10.1016/j.bej.2024.109496

Bai, B., Zhang, B., Chen, J., Feng, H. (2024), "Development of a natural inorganic diatomite curing agent on heavy metal-contaminated loess", *Phys. Chem. Earth.*, **136**, 103790. https://doi.org/10.1016/j.pce.2024.103790

Bai, B., Zhang, B., Chen, H., Chen, P. (2025), "A novel thermodynamic constitutive model of coarse-grained soils considering the particle breakage", *Transp. Geotech.*, **50**, 101462. https://doi.org/10.1016/j.trgeo.2024.101462

Bao, W., Liu, H., Wang, F., Du, J., Wang, Y., Li, H., Ye, X. (2024), "Keyhole critical failure criteria and variation rule under different thicknesses and multiple materials in K-TIG welding", *J. Manu. Proc.*, **126**, 48-59. https://doi.org/10.1016/j.jmapro.2024.07.093

Cao, Y., Xie, Z., Li, W., Wang, X., Wong, P.K., Zhao, J. (2024), "Combined path following and direct yaw-moment control for unmanned electric vehicles based on event-triggered T-S fuzzy method", *Int. J. Fuzzy Syst.* **26**, 2433-2448. https://doi.org/10.1007/s40815-024-01717-z

Chen, X., Shen, J., Bao, X., Wu, X., Tang, W., Cui, H. (2023), "A review of seismic resilience of shield tunnels", *Tunnell. Undergr. Space. Tech.* **136**, 105075. https://doi.org/10.1016/j.tust.2023.105075

Cheng, Y., Rabczuk, T., Ding, C. (2024), "Multi-DORGP for fast uncertainty quantification of multi-scale irregular defects in super large-scale fiber-reinforced composite", *Compos A Appl. Sci. Manuf.*, **182**, 108196 https://doi.org/10.1016/j.compositesa.2024.108196

Chu, S., Lin, M., Li, D., Lin, R., Xiao, S. (2025), "Adaptive

reward shaping based reinforcement learning for docking control of autonomous underwater vehicles", *Ocean. Eng.*, **318**, 120139. https://doi.org/10.1016/j.oceaneng.2024.120139

Chu, S., Xie, Z., Wong, P.K., Li, P., Li, W., Zhao, J. (2021), "Observer-based gain scheduling path following control for autonomous electric vehicles subject to time delay", *Vehicle. Syst. Dyn.*, **60**(5), 1602-1626. https://doi.org/10.1080/00423114.2020.1864419

Cong, F., Zhang, R., Li, W., Jin, Y., Yu, G., Wu, L. (2024), "Buckling analysis of moderately thick carbon fiber composite cylindrical shells under hydrostatic pressure", *Appl. Ocean. Res.*, **153**, 104272. https://doi.org/10.1016/j.apor.2024.104272

Deng, J., Liu, G., Wang, L., Liu, G., Wu, X. (2024), "Intelligent optimization design of squeeze casting process parameters based on neural network and improved sparrow search algorithm", *J. Indust. Inform. Integ.* **39**, 100600. https://doi.org/10.1016/j.jii.2024.100600

Deng, J., Liu, G., Wang, L., Liang, J., Dai, B. (2025), "An efficient extraction method of journal-article table data for data-driven applications", *Inform. Proc. Manag.*, **62**(3), 104006. https://doi.org/10.1016/j.ipm.2024.104006

Ding, H., Zhou, J. (2022), "Well-posedness of solutions for a class of quasilinear wave equations with strong damping and logarithmic nonlinearity", *Studies. Appl. Math.*, **149**(2), 441-486. https://doi.org/10.1111/sapm.12498

Dong, J.F., Liu, Y.C., Xu, Y., Yuan, S.C., Wang, Q.Y., Guan, Z.W., Chai, H.K. (2025), "Investigating the structural behaviour of double-skin steel tubes filled with basalt fibre reinforced recycled aggregate concrete under high temperature", *J. Building. Eng.*, **100**, 111782. https://doi.org/10.1016/j.jobe.2025.111782

Du, J., Liu, H., Wang, F., Bao, W., Li, H. (2024) "Solidification microstructure reconstruction and its effects on phase transformation, grain boundary transformation mechanism, and mechanical properties of TC4 alloy welded joint", *Metall. Mater. Trans. A.* **55**, 1193-1206. https://doi.org/10.1007/s11661-024-07317-8

Din, Q., Ishaque, W., Maqsood, I., Tounsi, A. (2023), "Discretization of laser model with bifurcation analysis and chaos control", *Adv. Nano. Res.* **15**(1), 25-34. https://doi.org/10.12989/anr.2023.15.1.025.

Das, T.K., Basak, S., Ganguly, S. (2024), "2D nanomaterial for microplastic Removal: A critical review", *Chem. Eng. J.*, **492**. https://doi.org/10.1016/j.cej.2024.152451

Feng, C., Kitipornchai, S., Yang, J. (2017), "Nonlinear bending of polymer nanocomposite beams reinforced with non-uniformly distributed graphene platelets (GPLs)", *Compos. Part B Eng.*, **110**, 132-140. https://doi.org/10.1016/j.compositesb.2016.11.024

Feng, G., Liu, T., Jiang, F., Guo, Z., Xiao, L., Wu, Q., Zhang, X., Hu, Q., Liu, J., Liang, J. (2024), "Novel (Ni, Mn) co-doping CuFe5O8 black ceramic pigment with pinning strengthen effect in high-temperature black zirconia ceramic application", *Ceram. Int.*, In Press. https://doi.org/10.1016/j.ceramint.2024.12.186

García-Macías, E., Rodríguez-Tembleque, L., Sáez, A. (2018), "Bending and free vibration analysis of functionally graded graphene vs. carbon nanotube reinforced composite plates", *Compos. Struct.*, **186**, 123-138. https://doi.org/10.1016/j.compstruct.2017.11.076

Guo, H., Zhuang, X., Rabczuk, T. (2019), "A deep collocation method for the bending analysis of kirchhoff plate", *Comput. Mater. Continua.*, **59**(2), 433-456. https://doi.org/10.32604/cmc.2019.06660.

Guo, Y., Maalla, A., Habibi, M., Moradi, Z. (2024), "Electroelastic wave dispersion in the rotary piezoelectric NEMS sensors/ actuators via nonlocal strain gradient theory", *Mech. Syst. Signal. Proc.*, **216**, 111453. https://doi.org/10.1016/j.ymssp.2024.111453

Ge, J., Hong, Y., Zeng, R., Li, Y., Habibi, M., (2023), "Increasing the attractiveness of physical education training with the involvement of nanotechnology, *Adv. Conc. Constr.* **16**(6), 291-302. https://doi.org/10.12989/acc.2024.16.6.291.

Ghosh, S.K., Nath, K., Ganguly, S.S., Das, T.K., Paul, S., Ghosh, T., Das, A.K., Das, N.C. (2023), "Improved rheological, barrier, antibacterial, and electromagnetic interference shielding properties of graphene and graphene derivatives based linear low density polyethylene nanocomposites", *Polym. Compos.*, **44**(9), 5702-5720. https://doi.org/10.1002/pc.27520,

Gao, J., Wu, Y., Shen, T. (2017), "A statistical combustion phase control approach of SI engines", *Mech. Syst. Signal. Proc.*, **85**, 218-235, https://doi.org/10.1016/j.ymssp.2016.08.007.

Gao, J., Feng, K., Wang, Y., Wu, Y., Chen, H. (2020), "Design, implementation and experimental verification of a compensator-based triple-step model reference controller for an automotive electronic throttle", *Control. Eng. Pract.*, **100**, 104447, https://doi.org/10.1016/j.conengprac.2020.104447.

He, X., Ding, J., Habibi, M., Safarpour, H., Safarpour, M. (2021), "Non-polynomial framework for bending responses of the multi-scale hybrid laminated nanocomposite reinforced circular/ annular plate", *Thin. Walled. Struct.*, **166**, 108019. https://doi.org/10.1016/j.tws.2021.108019

Huang, J., Pan, Z., Yang, S., Habibi, M., Safa, M. (2024), "Bending-based solution methodology using eigenvalue-eigenvector approach for analysis of foldable reinforced Golf Clubs cylindrical shell", *Mech. Adv. Mater. Struct.*, 1-14. https://doi.org/10.1080/15376494.2024.2378372

Han, D., Shi, J., Zhao, J., Wu, H., Zhou, Y., Li, L.H., Khan, M.K., Li, K.C. (2025), "LRCN: Layer-residual Co-Attention Networks for visual question answering", *Exp. Syst. Appl.*, **263**, 125658, https://doi.org/10.1016/j.eswa.2024.125658.

Huo, J., Zhang, G., Ghabussi, A., Habibi, M. (2021), "Bending analysis of FG-GPLRC axisymmetric circular/annular sector plates by considering elastic foundation and horizontal friction force using 3D-poroelasticity theory", *Compos. Struct.*, **276**, 114438. https://doi.org/10.1016/j.compstruct.2021.114438

Hou, T., Liu, X., Li, Z., Wang, Y., Chen, T. Huang, B. (2025), "Numerical investigation of cavitation induced noise and noise reduction mechanism for the leading-edge protuberances", *Appl. Ocean. Res.*, **154**, 104361. https://doi.org/10.1016/j.apor.2024.104361

Jermsittiparsert, K., Ghabussi, A., Forooghi, A., Shavalipour, A., Habibi, M., Jung, D.W., Safa, M. (2020), "Critical voltage, thermal buckling and frequency characteristics of a thermally affected GPL reinforced composite microdisk covered with piezoelectric actuator", *Mech. Based. Des. Struct. Mach.*, **50**(4), 331-1353. https://doi.org/10.1080/15397734.2020.1748052

Jin, Z., Huo, W., Habibi, M., Albaijan, I. (2024), "Thermo-foldable bending analysis of tunable shells using a higher-order modeling", *Mech. Adv. Mater. Struct.*, 1-14. https://doi.org/10.1080/15376494.2024.2369263

Jafari Mehrabadi, S., Sobhani Aragh, B., Khoshkhahesh, V., Taherpour, A. (2012), "Mechanical buckling of nanocomposite rectangular plate reinforced by aligned and straight single-walled carbon nanotubes", *Compos. Part B Eng.*, **43**(4), 2031-2040. https://doi.org/10.1016/j.compositesb.2012.01.067

Kadiri, A., Bendaida, M., Attia, A., Balubaid, M., Mahmoud, S. R., Bousahla, A.A., Tounsi, A. (2024), "Wave propagation in FG polymer composite nanoplates embedded in variable elastic medium", *Adv. Nano. Res.*, **17**(3), 235-248. https://doi.org/10.12989/anr.2024.17.3.235

Kumar, Y., Gupta, A., Tounsi, A. (2021) "Size-dependent vibration response of porous graded nanostructure with FEM and nonlocal continuum model", *Adv. Nano. Res.*, **11**(1), 1-17.

https://doi.org/10.12989/anr.2021.11.1.001

Ji, X., Jiang, P., Jiang, Y., Chen, H., Wang, W., Zhong, W., Zhang, X., Zhao, W., Zang, D. (2023), "Toward enhanced aerosol particle adsorption in never-bursting bubble via acoustic levitation and controlled liquid compensation", *Adv. Sci.*, **10**(19), 2300049. https://doi.org/10.1002/advs.202300049

Li, W., Xie, Z., Wong, P.K., Cao, Y., Hua, X., Zhao, J. (2019a), "Robust nonfragile H∞ optimum control for active suspension systems with time-varying actuator delay", *J. Vib. Control.*, **25**(18), 2435-2452. doi:10.1177/1077546319857338

Li, W., Xie, Z., Zhao, J., Wong, P.K., Li, P. (2019b), "Fuzzy finite-frequency output feedback control for nonlinear active suspension systems with time delay and output constraints", *Mech. Syst. Signal. Proc.*, **132**, 315-334. https://doi.org/10.1016/j.ymssp.2019.06.018

Li, W., Xie, Z., Wong, P. K., Ma, X., Cao, Y., Zhao, J. (2019c), "Nonfragile H∞ control of delayed active suspension systems in finite frequency under nonstationary running", *ASME. J. Dyn. Sys., Meas., Control.*, **141**(6), 061001. https://doi.org/10.1115/1.4042468

Li, W., Xie, Z., Zhao, J., Wong, P.K. (2020), "Velocity-based robust fault tolerant automatic steering control of autonomous ground vehicles via adaptive event triggered network communication", *Mech. Syst. Signal. Proc.*, **143**, 106798. https://doi.org/10.1016/j.ymssp.2020.106798.

Li, W., Xie, Z., Cao, Y., Wong, P.K., Zhao, J. (2021a), "Sampled-data asynchronous fuzzy output feedback control for active suspension systems in restricted frequency domain", *IEEE/CAA. J. Automat. Sin.*, **8**(5), 1052-1066 https://doi.org/10.1109/JAS.2020.1003306.

Li, W., Xie, Z., Zhao, J., Wong, P. K., Wang, H., Wang, X. (2021b), "Static-output-feedback based robust fuzzy wheelbase preview control for uncertain active suspensions with time delay and finite frequency constraint", *IEEE/CAA. J. Automat. Sin.*, **8**(3), 664-678 https://doi.org/10.1109/JAS.2020.1003183.

Li, W., Xie, Z., Wong, P.K., Mei, X., Zhao, J. (2021c), "Adaptive-event-trigger-based fuzzy nonlinear lateral dynamic control for autonomous electric vehicles under insecure communication networks", *IEEE. Trans. Ind. Electron.*, **68**(3), 2447-2459. https://doi.org/10.1109/TIE.2020.2970680.

Li, W., Xie, Z., Zhao, J., Gao, J., Hu, Y., Wong, P.K. (2022a), "Human-machine shared steering control for vehicle lane keeping systems via a fuzzy observer-based event-triggered method", *IEEE. T. Intel. Transp. Syst.*, **23**(8), 13731-13744. https://doi.org/10.1109/TITS.2021.3126876.

Li, Y., Li, S., Guo, K., Fang, X., Habibi, M. (2022b), "On the modeling of bending responses of graphene-reinforced higher order annular plate via two-dimensional continuum mechanics approach", *Eng. Comput.*, **38**(1), 703-724. https://doi.org/10.1007/s00366-020-01166-w

Li, N., Hu, X., Lu, Y., Li, Y., Ren, M., Luo, X., Ji, Y., Chen, Q., Sui, X. (2024a) "Wavelength-selective near-infrared organic upconversion detectors for miniaturized light detection and visualization", *Adv. Funct. Mater.*, **34**(51), 2411626. https://doi.org/10.1002/adfm.202411626

Li, H., Li, Y., Zhang, G., Liu, Y., Han, Z., Zhang, H., Xu, Q., Zhao, J., Jin, M., Song, D., Sun, M., Wang, F., Zhu, X., Lan, H (2024b), "Directly printing high-resolution, high-performance 3D curved electronics based on locally polarized electric-field-driven vertical jetting", *Addit. Manuf.*, **96**, 104579, https://doi.org/10.1016/j.addma.2024.104579.

Li, J., Wu, Z., Habibi, M., Albaijan, I. (2024c), "An inspection of the metal-foam beam considering torsional dynamic responses, *Solid. State. Com.*, **391**, 115638. https://doi.org/10.1016/j.ssc.2024.115638

Liu, D., Li, Z., Kitipornchai, S., Yang, J. (2019), "Three-dimensional free vibration and bending analyses of functionally graded graphene nanoplatelets-reinforced nanocomposite annular plates", *Compos. Struct.*, **229**, 111453. https://doi.org/10.1016/j.compstruct.2019.111453

Liang, Z., Zhao, Y., Yu, H., Habibi, M., Mahmoudi, T. (2024a), "Artificial neural networks coupled with numerical approach for the stability prediction of non-uniform functionally graded microscale cylindrical structures, *Structures*, **60**, 105826. https://doi.org/10.1016/j.istruc.2023.105826

Liang, K., Sun, P., Wang, D. (2024b), "Quantitative analysis of deformation performance for skew slab based on deformation energy decomposition method of triangular prism element", *Structures*, **63**, 106447. https://doi.org/10.1016/j.istruc.2024.106447

Long, X., Li, Y., Shen, Z., Su, Y., Gu, T., Siow, K.S. (2024), "Review of uniqueness challenge in inverse analysis of nano-indentation", *J. Manu. Proc.*, **131**, 1897-1916. https://doi.org/10.1016/j.jmapro.2024.10.005

Luo, Y., Zhang, H., Chen, Z., Li, Q., Ye, S., Liu, Q. (2024), "Novel multidimensional composite development for aging resistance of SBS-modified asphalt by attaching zinc oxide on expanded vermiculite", *Energy Fuels*, **38**(170), 16772-16781. https://doi.org/10.1021/acs.energyfuels.4c02685.

Luo, Y.X., Dong, Y.L. (2024), "Strain measurement at up to 3000 °C based on Ultraviolet-Digital Image Correlation", *NDT E Int.*, **146**, 103155. https://doi.org/10.1016/j.ndteint.2024.103155.

Lu, L., Liao, K., Habibi, M., Safarpour, H., Elhosiny, Ali, H. (2023), "Numerical methods to predict aero thermally induced vibrations of a curved pipe structure reinforced by GPLs", *Structures*, **55**, 1607-1621. https://doi.org/10.1016/j.istruc.2023.06.105

Liu, H., Zhao, Y., Pishbin, M., Habibi, M., Bashir, M.O., Issakhov, A. (2022a), "A comprehensive mathematical simulation of the composite size-dependent rotary 3D microsystem via two-dimensional generalized differential quadrature method", *Eng. Comput.* **38**(5), 4181-4196. https://doi.org/10.1007/s00366-021-01419-2

Liu, J., Xie, Z., Gao, J., Hu, Y., Zhao, J. (2022b), "Failure characteristics of the active-passive damping in the functionally graded piezoelectric layers-magnetorheological elastomer sandwich structure", *Int. J. Mech. Sci.*, **215**, 106944. https://doi.org/10.1016/j.ijmecsci.2021.106944

Lv, H., Zeng, J., Zhu, Z., Dong, S., Li, W. (2024a), "Study on prestress distribution and structural performance of heptagonal six-five-strut alternated cable dome with inner hole", *Structures*, **65**, 106724, https://doi.org/10.1016/j.istruc.2024.106724.

Lv, S., Liu, H., Wang, F., Liu, X., Peng, M., Wei, Y., Li, C. (2024b), "Effect of axial misalignment on the microstructure, mechanical, and corrosion properties of magnetically impelled arc butt welding joint", *Mater. Today Commun.*, **40**, 109866. https://doi.org/10.1016/j.mtcomm.2024.109866

Lori Dehsaraji, M., Arefi, M., Loghman, A., (2021), "Size dependent free vibration analysis of functionally graded piezoelectric micro/nano shell based on modified couple stress theory with considering thickness stretching effect", *Def. Tech.*, **17**(1), 119-134. https://doi.org/10.1016/j.dt.2020.01.001.

Mohammadi, M., Arefi, M., Dimitri, R., Tornabene, F. (2019), "Higher-order thermo-elastic analysis of FG-CNTRC cylindrical vessels surrounded by a Pasternak foundation", *Nanomaterials* **9**(1), 79. https://doi.org/10.3390/nano9010079

Ma, K., Xie, Z., Wong, P.K., Li, W., Chu, S., Zhao, J. (2022), "Robust Takagi-Sugeno fuzzy fault tolerant control for vehicle lateral dynamics stabilization with integrated actuator fault and time delay", *J. Dyn. Sys., Meas., Control.*, **144**(2), 021002. https://doi.org/10.1115/1.4052273

Ma, B., Chen, K.Y., Habibi, M., Albaijan, I. (2023), "Static/ dynamic analyses of sandwich micro-plate based on modified

strain gradient theory", *Mech. Adv. Mater. Struct.*, **31**(23), 5760-5767. https://doi.org/10.1080/15376494.2023.2219453

Meng, F., Pang, A., Dong, X., Han, C., Sha, X. (2018), "H∞ optimal performance design of an unstable plant under bode integral constraint", *Complexity*, **2018**(1), 4942906. https://doi.org/10.1155/2018/4942906

Meng, F., Wang, D., Yang, P., Xie, G. (2019), "Application of sum of squares method in nonlinear h∞ control for satellite attitude maneuvers", *Complexity*, **2019**(1), 5124108. https://doi.org/10.1155/2019/5124108

Meng, S., Meng, F., Zhang, F., Li, Q., Zhang, Y., Zemouche, A. (2024), "Observer design method for nonlinear generalized systems with nonlinear algebraic constraints with applications", *Automatica*, **162**, 111512. https://doi.org/10.1016/j.automatica.2024.111512.

Madenci, E., Özkiliç, Y.O., Hakamy, A., Tounsi, A. (2023), "Experimental tensile test and micro-mechanic investigation on carbon nanotube reinforced carbon fiber composite beams", *Adv. Nano. Res.* **14**(5), 443-450. https://doi.org/10.12989/anr.2023.14.5.443.

Mohammadimehr, M., Rostami, R., Arefi, M. (2016), "Electro-elastic analysis of a sandwich thick plate considering FG core and composite piezoelectric layers on Pasternak foundation using TSDT", *Steel. Compos. Struct.* **20**(3), 513-543. https://doi.org/10.12989/scs.2016.20.3.513

Mehar, K., Panda, S.K. (2018), "Elastic bending and stress analysis of carbon nanotube-reinforced composite plate: Experimental, numerical, and simulation", *Adv. Poly. Tech.*, **37**, 1643-1657. https://doi.org/10.1002/adv.21821.

Nam, V.B, Zhuang, X., Rabczuk. T. (2019), "Uncertainty quantification for mechanical properties of polyethylene based on fully atomistic model", *Materials*, **12**(21), 3613. https://doi.org/10.3390/ma12213613

Ni, Z.L., Li, B.H., Nazarov, A.A., Ma, J.S., Yuan, Z.P., Wang, X. X., Li, H. (2024), "Simulation of ultrasonic welding of Cu/Cu joints with an interlayer of Cu nanoparticles", *Mater. Today. Com.*, **39**, 109330. https://doi.org/10.1016/j.mtcomm.2024.109330

Peng, S., Habibi, M., Pourjabari, A. (2023), "Generalized differential quadrature element solution, swarm, and GA optimization technique to obtain the optimum frequency of the laminated rotary nanostructure", *Eng. Anal. Bound. Elem.*, **151**, 101-114. https://doi.org/10.1016/j.enganabound.2023.02.052

Rahimi, G.H., Arefi, M., Khoshgoftar, M.J. (2012), "Electro elastic analysis of a pressurized thick-walled functionally graded piezoelectric cylinder using the first order shear deformation theory and energy method", *Mechanika*, **18**(3), 292-300. https://doi.org/10.5755/j01.mech.18.3.1875.

Ren, F., Liu, X., Charles, V., Zhao, X., Balsalobre-Lorente, D. (2025), "Integrated efficiency and influencing factors analysis of ESG and market performance in thermal power enterprises in China: A hybrid perspective based on parallel DEA and a benchmark model", *Energy. Econom.*, **141**, 108138, https://doi.org/10.1016/j.eneco.2024.108138.

Samadzadeh, M.H., Arefi, M., Loghman, A. (2024), "Static bending analysis of pressurized cylindrical shell made of graphene origami auxetic metamaterials based on higher-order shear deformation theory", *Heliyon*, **10**(16), e36319. https://doi.org/10.1016/j.heliyon.2024.e36319.

Sekkak, M., Zerrouki, R., Zidour, M., Tounsi, A., Bourada, M., Selim, M.M., Saad, H.A. (2024) "Static analysis of nonlinear FG-CNT reinforced nano-composite beam resting on Winkler/ Pasternak foundation", *Adv. Nano. Res.*, **16**(5), 509-519. https://doi.org/10.12989/anr.2024.16.5.509.

Samaniego, E., Anitescu, C., Goswami, S., Nguyen-Thanh, V.M. Guo, H., Hamdia, K., Zhuang, X., Rabczuk, T. (2020), "An energy approach to the solution of partial differential equations in computational mechanics via machine learning: Concepts, implementation and applications", *Comput. Meth. Appl. Mech. Eng.* **362**(15), 112790 https://doi.org/10.1016/j.cma.2019.112790.

Song, M., Yang, J., Kitipornchai, S. (2018), "Bending and buckling analyses of functionally graded polymer composite plates reinforced with graphene nanoplatelets", *Compos. Part B Eng.*, **134**, 106-113. https://doi.org/10.1016/j.compositesb.2017.09.043

Shen, H.S. (2009), "Nonlinear bending of functionally graded carbon nanotube-reinforced composite plates in thermal environments", *Compos. Struct.*, **91**,1), 9-19. https://doi.org/10.1016/j.compstruct.2009.04.026

Shen, Z., Dong, R., Li, J., Su, Y., Long, X. (2024), "Determination of gradient residual stress for elastoplastic materials by nanoindentation", *J. Manu. Proc.*, **109**, 359-366. https://doi.org/10.1016/j.jmapro.2023.10.030

Shen, J., Bao, X., Li, J., Chen, X., Cui, H. (2025), "Study on the mechanism of EPWP dissipation at the joints of shield tunnel in liquefiable strata during seismic events", *Soil. Dyn. Earthq. Eng.*, **188**, Part A, 109089. https://doi.org/10.1016/j.soildyn.2024.109089

Sun, B. L., Shi, X. L., Hu, Q., Du, M., Gong, H., Wang, J., Fan, Y., Zhang, J., Li, Z. (2024), "Ultrahigh-strength textile fiber-supported schiff base copper complexes for photocatalytic degradation of methyl orange", *ACS. Appl. Polym. Mater.*, **6**(21), 13077-13088. https://doi.org/10.1021/acsapm.4c02009

Shi, X., Li, J., Habibi, M. (2022), "On the statics and dynamics of an electro-thermo-mechanically porous GPLRC nanoshell conveying fluid flow", *Mech. Based. Des. Struct.*, **50**(6), 2147-2183. https://doi.org/10.1080/15397734.2020.1772088

Shi, J., Zhao, B., Niu, X., Xin, Q., Xu, H., Lu, X. (2024), "Time-varying dynamic characteristic analysis of journal-thrust coupled bearings based on the transient lubrication considering thermal-pressure coupled effect", *Phys. Fluids.*, **36**(8), 083116. https://doi.org/10.1063/5.0217495

Song, G., Zou, Y., Nie, Y., Habibi, M., Albaijan, I., Toghroli, E. (2024), "Application of Hashin-Shtrikman bounds homogenization model for frequency analysis of imperfect FG bio-composite plates", *J. Mech. Beh. Biomed. Mater.*, **151**, 106321. https://doi.org/10.1016/j.jmbbm.2023.106321

Tlidji, Y., Benferhat, R., Daouadji, T.H., Tounsi, A., Cong Trinh, L. (2022), "Free vibration analysis of FGP nanobeams with classical and non-classical boundary conditions using State-space approach", *Adv. Nano. Res.* **13**(5), 453-463. https://doi.org/10.12989/anr.2022.13.5.453.

Tao, C., Dai. T. (2022), "Modified couple stress-based nonlinear static bending and transient responses of size-dependent sandwich microplates with graphene nanocomposite and porous layers", *Thin. Walled. Struct.*, **171**, 108704. https://doi.org/10.1016/j.tws.2021.108704

Thai, C.H., Ferreira, A.J.M., Tran, T.D., Phung-Van, P. (2019), "Free vibration, buckling and bending analyses of multilayer functionally graded graphene nanoplatelets reinforced composite plates using the NURBS formulation", *Compos. Struct.*, **220**, 749-759. https://doi.org/10.1016/j.compstruct.2019.03.100

Tian, R., Guan, H., Lu, X., Zhang, X., Hao, H., Feng, W., Zhang, G. (2023), "Dynamic crushing behavior and energy absorption of hybrid auxetic metamaterial inspired by Islamic motif art", *Appl. Math. Mech. Eng. Ed.*, **44**(3), 345-362. https://doi.org/10.1007/s10483-023-2962-9

Vali, H., Arefi, M. (2023), "Extension of a novel higher order modeling to the vibration responses of sandwich graphene origami cylindrical panel", *Arch. Civil Mech. Eng.*, **23**, 268. https://doi.org/10.1007/s43452-023-00797-2

Xie, Z., You, W., Wong, P.K., Li, W., Ma, X., Zhao, J. (2023),

"Robust fuzzy fault tolerant control for nonlinear active suspension systems via adaptive hybrid triggered scheme", *Int. J. Adapt. Control. Signal. Proc.*, **37**, 1608-1627.

Xie, Z., You, W., Wong, P.K., Li, W., Zhao, J. (2024a), "Fuzzy robust non-fragile control for nonlinear active suspension systems with time varying actuator delay", *Proc. Inst. Mech. Eng. Part D J. Automobile Eng.*, **238**(1), 46-62. https://doi.org/10.1177/09544070221125528

Xie, J., Wen, M., Ding, P., Tu, Y., Wu, D., Liu, K., Chen, M. (2024b), "One-dimensional consolidation analysis of layered unsaturated soils: An improved model integrating interfacial flow and air contact resistance effects", *Comput. Geotech.*, **176**, 106791. https://doi.org/10.1016/j.compgeo.2024.106791

Xu, Y., Xie, Z., Zhao, J., Li, W., Li, P. Wong, P.K. (2021), "Robust non-fragile finite frequency H∞ control for uncertain active suspension systems with time-delay using T-S fuzzy approach", *J. Franklin. Inst.*, **358**(8), 4209-4238. https://doi.org/10.1016/j.jfranklin.2021.03.019

Xiao, H., Habibi, M., Habibi, M. (2024), "Bulk wave propagation analysis of imperfect FG bio-composite beams resting on variable elastic medium", *Mater. Today. Commun*, **39**, 108524. https://doi.org/10.1016/j.mtcomm.2024.108524.

Yang, N., Zou, Y., Arefi, M. (2024), "Bending results of graphene origami reinforced doubly curved shell", *Def. Tech.*, **35**, 198-210. https://doi.org/10.1016/j.dt.2023.11.017

Yu, C., Lin, P., Wu, Z., Habibi, M., Zhang, W. (2024a), "Multi-load effect on the deformation analysis of composite nano reinforced origami sandwich panel", *Mech. Adv. Mater. Struct.* 1-19. https://doi.org/10.1080/15376494.2024.2367015

Yu, Z., Zhao, J., Markov, V., Han, D. (2024b), "Energy Effects of hydrogen addition on ignition characteristics and engine performance of ammonia-hydrogen blended fuel: A kinetic analysis", *Int. J. Hydrogen. Energy.*, **87**, 722-735. https://doi.org/10.1016/j.ijhydene.2024.09.073

Ye, J., Gao, Y., Gao, H., Zhao, Q., Xu, D., Zhou, M., Shi. M., Xue, X. (2025), "Effects of pristine and photoaged tire wear particles and their leachable additives on key nitrogen removal processes and nitrous oxide accumulation in estuarine sediments", *J. Hazard. Mater.*, **487**, 137136. https://doi.org/10.1016/j.jhazmat.2025.137136

Yin, J., Zou, Y., Li, J., Zhang, W., Li, X., Habibi, M. (2024), "Dynamic stability and frequency responses of the tilted curved nanopipes in a supersonic airflow via 2D hybrid nonlocal strain gradient theory, *Eng. Struct.*, **301**, 117240. https://doi.org/10.1016/j.engstruct.2023.117240

Wang, A., Chen, H., Hao, Y., Zhang, W. (2018), "Vibration and bending behavior of functionally graded nanocomposite doubly-curved shallow shells reinforced by graphene nanoplatelets", *Result. Phys.*, **9**, 550-559. https://doi.org/10.1016/j.rinp.2018.02.062

Wang, Y., Xie, K., Fu, T., Shi, C. (2019), "Bending and elastic vibration of a novel functionally graded polymer nanocomposite beam reinforced by graphene nanoplatelets", *Nanomaterials*, **9**, 1690. https://doi.org/10.3390/nano9121690

Wang, Y., Wang, J., Cai, R., Zhang, J., Xia, S., Li, Z., Yu, C., Wu, Y. (2024a), "Enhanced local CO coverage on Cu quantum dots for boosting electrocatalytic CO2 reduction to ethylene", *Adv. Func. Mater.*, 2417764. https://doi.org/10.1002/adfm.202417764.

Wang, W., Zhang, J., Habibi, M., Albaijan, I. (2024b), "Stretchable-thickness model for dynamic responses of graphene origami reinforced badminton sport plate", *Mech. Adv. Mater. Struct.*, 1-13. https://doi.org/10.1080/15376494.2024.2373976

Wang, Z., Yuan, Y., Zhang, S., Lin, Y., Tan, J. (2024c), "A multi-state fusion informer integrating transfer learning for metal tube bending early wrinkling prediction", *Appl. Soft. Comput.*, **151**, 110991. https://doi.org/10.1016/j.asoc.2023.110991

Wang, Z., Wang, C., Zhang, S., Qiu, L., Lin, Y., Tan, J., Sun, C. (2024d), "Towards high-accuracy axial springback: Mesh-based simulation of metal tube bending via geometry/process-integrated graph neural networks", *Exp. Syst. Appl.*, **255**, 124577. https://doi.org/10.1016/j.eswa.2024.124577

Wang, C., Song, Z., Fan, H. (2024e), "Novel evidence theory-based reliability analysis of functionally graded plate considering thermal stress behavior", *Aer. Sci. Tech.*, **146**, 108936. https://doi.org/10.1016/j.ast.2024.108936

Wang, X., Zhang, Y., Wen, M., Mang, H.A. (2025), "A simple hybrid linear and nonlinear interpolation finite element for the adaptive Cracking Elements Method", *Finite. Elem. Anal. Des.*, **244**, 104295 https://doi.org/10.1016/j.finel.2024.104295.

Wu, J., Habibi, M. (2022), "Dynamic simulation of the ultra-fast-rotating sandwich cantilever disk via finite element and semi-numerical methods", *Eng. Comput.*, **38**(50), 4127-4143. https://doi.org/10.1007/s00366-021-01396-6

Wei, J., Fan, P., Huang, Y., Zeng, H., Jiang, R., Wu, Z., Zhang, Y., Hu, Z. (2024), "(±)- Hypandrone A, a pair of polycyclic polyprenylated acylphloroglucinol enantiomers with a caged 7/6/5/6/6 pentacyclic skeleton from Hypericum androsaemum", *Org. Chem. Front.*, **12**(11), 3459-3464. https://doi.org/10.1039/D4QO00444B.

Zha, J., Zhang, Z. (2024), "Reversible negative compressibility metamaterials inspired by Braess's Paradox", *Smart. Mater. Struct.*, **33**(7), 075036. https://doi.org/10.1088/1361-665X/ad59e6

Zhang, T., Shi, X. L., Hu, Q., Gong, H., Shi, K., Li, Z. (2024a), "Ultrahigh-performance fiber-supported iron-based ionic liquid for synthesizing 3,4-Dihydropyrimidin-2-(1H)-ones in a cleaner manner", *Langmuir*, **40**(18), 9579-9591. https://doi.org/10.1021/acs.langmuir.4c00332

Zhang, Y., Xu, L., Wang, J., Pan, H., Dou, M., Teng, Y., Fu, X., Liu, Z., Huang, X., Wang, M. (2024b), "Bagasse-based porous flower-like MoS2/carbon composites for efficient microwave absorption", *Carbon Lett.*, 1-16. https://doi.org/10.1007/s42823-024-00832-z

Zhang, Q., Xie, M., Zhou, D., Habibi, M., Khorami, M. (2024c), "Bending responses of graphene nanoplatelets reinforced sandwich cylindrical micro panel with piezoelectric layers", *Mech. Adv. Mater. Struct.*, 1-16. https://doi.org/10.1080/15376494.2024.2385008

Zhang, Z., Fan, W., Long, Y., (2024d) "Hybrid-driven origami gripper with variable stiffness and finger length", *Cyborg Bionic Syst.*, **5**, 0103. https://doi.org/10.34133/cbsystems.0103

Zhang, M., Zhou, S., Huang, R., Xu, F., Wang, J., Dai, S., Zhang, Y., Zhu, L. (2025a), "Cold sprayed Cu-coated AlN reinforced copper matrix composite coatings with improved tribological and anticorrosion properties", *Surf. Coatings. Tech.*, **496**, 131666. https://doi.org/10.1016/j.surfcoat.2024.131666

Zhang, M., Xu, Y.C., Wang, J.F. (2025b), "Cold-sprayed Cu matrix composite coatings with core-shell structured Co@WC reinforcements on Q235 steel", *Surf. Interf.*, **56**, 105577. https://doi.org/10.1016/j.surfin.2024.105577

Zhou, C., Zhao, Y., Zhang, J., Fang, Y., Habibi M., (2020), "Vibrational characteristics of multi-phase nanocomposite reinforced circular/annular system", *Adv. Nano. Res.*, **9**(4), 295-307. https://doi.org/10.12989/anr.2020.9.4.295

Zhou, L., Riska, K., Ji, C. (2017), "Simulating transverse icebreaking process considering both crushing and bending failures", *Marine. Struct.*, **54**, 167-187. https://doi.org/10.1016/j.marstruc.2017.04.004

Zhou, L., Gao, J., Xu, S., Bai, X. (2018), "A numerical method to simulate ice drift reversal for moored ships in level ice", *Cold. Reg. Sci. Tech.*, **152**, 35-47. https://doi.org/10.1016/j.coldregions.2018.04.008

Zghal, S., Frikha, A., Dammak, F. (2018), "Non-linear bending analysis of nanocomposites reinforced by graphene-nanotubes with finite shell element and membrane enhancement", *Eng. Struct.*, **158**, 95-109. https://doi.org/10.1016/j.engstruct.2017.12.017.

Zhao, Z. Feng, C. Wang, Y. Yang, J. (2017), "Bending and vibration analysis of functionally graded trapezoidal nanocomposite plates reinforced with graphene nanoplatelets (GPLs)", *Compos. Struct.*, **180**, 799-808. https://doi.org/10.1016/j.compstruct.2017.08.044

Zhuang, X., Guo, H., Alajlan, N., Zhu, H., Rabczuk, T. (2021), "Deep autoencoder based energy method for the bending, vibration, and buckling analysis of Kirchhoff plates with transfer learning", *Eur. J. Mech. A Solids* **87**, 104225. https://doi.org/10.1016/j.euromechsol.2021.104225.

Zhao, J., Wong, P. K., Xie, Z., Ma, X., Hua, X. (2019) "Design and control of an automotive variable hydraulic damper using cuckoo search optimized pid method", *Int. J Automot. Technol.*, **20**, 51-63. https://doi.org/10.1007/s12239-019-0005-z

Zhang, M., Jiang, X. Arefi, M. (2023), "Dynamic formulation of a sandwich microshell considering modified couple stress and thickness-stretching", *Eur. Phys. J. Plus.*, **138**, 227. https://doi.org/10.1140/epjp/s13360-023-03753-4

Zhu, L., Ren, H., Habibi, M., Mohammed, K.J., Khadimallah, M.A. (2022), "Predicting the environmental economic dispatch problem for reducing waste nonrenewable materials via an innovative constraint multi-objective Chimp Optimization Algorithm", *J. Clean. Prod.*, **365**, 132697. https://doi.org/10.1016/j.jclepro.2022.132697

Zhiqiang, S., Aiyun, L., Daichang, Z., Shuangjun, L., Habibi, M., Xiaoling, F., Albaijan, I. (2024), "Application of a folded nanostructure reinforcement for the pole vault curved shell", *Mech. Adv. Mater. Struct.*, 1-15. https://doi.org/10.1080/15376494.2024.2375368

JL

Appendix

$$\{\mathfrak{V}_1,\mathfrak{V}_2,\mathfrak{V}_3\} = \int_{-h/2}^{+h/2}\left(1+\frac{\mathcal{Z}}{R_y}\right)\frac{\mathbb{E}}{1-\vartheta^2}\left\{\frac{1}{R_x\left(1+\frac{\mathcal{Z}}{R_x}\right)},\frac{1}{R_x},\frac{\mathcal{Z}}{R_x\left(1+\frac{\mathcal{Z}}{R_x}\right)}\right\}d\mathcal{Z}$$

$$\{\mathfrak{V}_4,\mathfrak{V}_5,\mathfrak{V}_6\} = \int_{-h/2}^{+h/2}\left(1+\frac{\mathcal{Z}}{R_y}\right)\frac{\mathbb{E}\vartheta}{1-\vartheta^2}\left\{\frac{1}{R_y\left(1+\frac{\mathcal{Z}}{R_y}\right)},\frac{1}{R_y},\frac{\mathcal{Z}}{R_y\left(1+\frac{\mathcal{Z}}{R_y}\right)}\right\}d\mathcal{Z}$$

$$\{\mathcal{R}_X^{1T},\mathcal{R}_X^{2T},\mathcal{R}_X^{3T}\} = \int_{-h/2}^{+h/2}\left(1+\frac{\mathcal{Z}}{R_y}\right)\frac{\mathbb{E}}{1-\vartheta}\alpha\mathcal{T}\left\{1,\left(1+\frac{\mathcal{Z}}{R_x}\right),\mathcal{Z}\right\}d\mathcal{Z}$$

$$\{\mathcal{R}_X^{4T},\mathcal{R}_X^{5T},\mathcal{R}_X^{6T}\} = \int_{-h/2}^{+h/2}\left(1+\frac{\mathcal{Z}}{R_x}\right)\frac{\mathbb{E}}{1-\vartheta}\alpha\mathcal{T}\left\{1,\left(1+\frac{\mathcal{Z}}{R_y}\right),\mathcal{Z}\right\}d\mathcal{Z}$$

$$\{\mathfrak{V}_8,\mathfrak{V}_9,\mathfrak{V}_{10}\} = \int_{-h/2}^{+h/2}\left(1+\frac{\mathcal{Z}}{R_y}\right)\left(1+\frac{\mathcal{Z}}{R_x}\right)\frac{\mathbb{E}}{1-\vartheta^2}\left\{\frac{1}{R_x\left(1+\frac{\mathcal{Z}}{R_x}\right)},\frac{1}{R_x},\frac{\mathcal{Z}}{R_x\left(1+\frac{\mathcal{Z}}{R_x}\right)}\right\}d\mathcal{Z}$$

$$\{\mathfrak{V}_{11},\mathfrak{V}_{12},\mathfrak{V}_{13}\} = \int_{-h/2}^{+h/2}\left(1+\frac{\mathcal{Z}}{R_y}\right)\left(1+\frac{\mathcal{Z}}{R_x}\right)\frac{\mathbb{E}\vartheta}{1-\vartheta^2}\left\{\frac{1}{R_y\left(1+\frac{\mathcal{Z}}{R_y}\right)},\frac{1}{R_y},\frac{\mathcal{Z}}{R_y\left(1+\frac{\mathcal{Z}}{R_y}\right)}\right\}d\mathcal{Z}$$

$$\{\mathfrak{V}_{15},\mathfrak{V}_{16},\mathfrak{V}_{17}\} = \int_{-h/2}^{+h/2}\left(1+\frac{\mathcal{Z}}{R_y}\right)\mathcal{Z}\frac{\mathbb{E}}{1-\vartheta^2}\left\{\frac{1}{R_y\left(1+\frac{\mathcal{Z}}{R_y}\right)},\frac{1}{R_y},\frac{\mathcal{Z}}{R_y\left(1+\frac{\mathcal{Z}}{R_y}\right)}\right\}d\mathcal{Z}$$

$$\{\mathfrak{V}_{18},\mathfrak{V}_{19},\mathfrak{V}_{20}\} = \int_{-h/2}^{+h/2}\left(1+\frac{\mathcal{Z}}{R_y}\right)\mathcal{Z}\frac{\mathbb{E}\vartheta}{1-\vartheta^2}\left\{\frac{1}{R_y\left(1+\frac{\mathcal{Z}}{R_y}\right)},\frac{1}{R_y},\frac{\mathcal{Z}}{R_y\left(1+\frac{\mathcal{Z}}{R_y}\right)}\right\}d\mathcal{Z}$$

$$\{\mathfrak{V}_{22},\mathfrak{V}_{23},\mathfrak{V}_{24}\} = \int_{-h/2}^{+h/2}\left(1+\frac{\mathbb{Z}}{R_\zeta}\right)\frac{\mathbb{E}}{1-\vartheta^2}\left\{\frac{1}{R_x\left(1+\frac{\mathcal{Z}}{R_x}\right)},\frac{1}{R_x},\frac{\mathcal{Z}}{R_x\left(1+\frac{\mathcal{Z}}{R_x}\right)}\right\}d\mathcal{Z}$$

$$\{\mathfrak{V}_{25},\mathfrak{V}_{26},\mathfrak{V}_{27}\} = \int_{-h/2}^{+h/2}\left(1+\frac{\mathcal{Z}}{R_y}\right)\left(1+\frac{\mathcal{Z}}{R_x}\right)\frac{\mathbb{E}}{1-\vartheta^2}\left\{\frac{1}{R_x\left(1+\frac{\mathcal{Z}}{R_x}\right)},\frac{1}{R_x},\frac{\mathcal{Z}}{R_x\left(1+\frac{\mathcal{Z}}{R_x}\right)}\right\}d\mathcal{Z}$$

$$\{\mathfrak{V}_{28},\mathfrak{V}_{29},\mathfrak{V}_{30}\} = \int_{-h/2}^{+h/2}\left(1+\frac{\mathcal{Z}}{R_y}\right)\mathcal{Z}\frac{\mathbb{E}}{1-\vartheta^2}\left\{\frac{1}{R_x\left(1+\frac{\mathcal{Z}}{R_x}\right)},\frac{1}{R_x},\frac{\mathcal{Z}}{R_x\left(1+\frac{\mathcal{Z}}{R_x}\right)}\right\}d\mathcal{Z}$$

$$\{\mathfrak{V}_{31},\mathfrak{V}_{32},\mathfrak{V}_{33}\} = \int_{-h/2}^{+h/2}\left(1+\frac{\mathcal{Z}}{R_x}\right)\frac{\mathbb{E}}{2(1+\vartheta)}\left\{1,\frac{1}{R_y\left(1+\frac{\mathcal{Z}}{R_y}\right)},\frac{1}{R_x}\right\}d\mathcal{Z}$$

$$\{\mathfrak{V}_{35},\mathfrak{V}_{36},\mathfrak{V}_{37}\} = \int_{-h/2}^{+h/2}\left(1+\frac{\mathcal{Z}}{R_x}\right)\frac{\mathbb{E}}{2(1+\vartheta)}\left\{1,\frac{1}{R_x\left(1+\frac{\mathcal{Z}}{R_x}\right)},\frac{1}{R_y}\right\}d\mathcal{Z}$$

$$\{\mathfrak{V}_{39},\mathfrak{V}_{40},\mathfrak{V}_{41}\} = \int_{-h/2}^{+h/2}\left(1+\frac{\mathcal{Z}}{R_x}\right)\left(1+\frac{\mathcal{Z}}{R_y}\right)\frac{\mathbb{E}}{2(1+\vartheta)}\left\{1,\frac{1}{R_y\left(1+\frac{\mathcal{Z}}{R_y}\right)},\frac{1}{R_x}\right\}d\mathcal{Z}$$

$$\{\mathfrak{V}_{43},\mathfrak{V}_{44},\mathfrak{V}_{45}\} = \int_{-h/2}^{+h/2}\left(1+\frac{\mathcal{Z}}{R_x}\right)\left(1+\frac{\mathcal{Z}}{R_y}\right)\frac{\mathbb{E}}{2(1+\vartheta)}\left\{1,\frac{1}{R_x\left(1+\frac{\mathcal{Z}}{R_x}\right)},\frac{1}{R_y}\right\}d\mathcal{Z}$$

$$\{\mathfrak{V}_{47},\mathfrak{V}_{48},\mathfrak{V}_{49},\mathfrak{V}_{50},\mathfrak{V}_{51},\mathfrak{V}_{52}\} = \int_{-h/2}^{+h/2}\left(1+\frac{\mathcal{Z}}{R_y}\right)\frac{\mathbb{E}}{2(1+\vartheta)}\begin{Bmatrix}\frac{1}{R_x\left(1+\frac{\mathcal{Z}}{R_x}\right)},\frac{1}{R_y\left(1+\frac{\mathcal{Z}}{R_y}\right)},\mathcal{Z}\frac{1}{R_x\left(1+\frac{\mathcal{Z}}{R_x}\right)},\\ \mathcal{Z}\frac{1}{R_y\left(1+\frac{\mathcal{Z}}{R_y}\right)},\mathcal{Z}\frac{1}{2}\left(\frac{1}{R_x}-\frac{1}{R_y}\right)\frac{1}{R_x\left(1+\frac{\mathcal{Z}}{R_x}\right)},\\ \mathcal{Z}\frac{1}{2}\left(\frac{1}{R_x}-\frac{1}{R_y}\right)\frac{1}{R_y\left(1+\frac{\mathcal{Z}}{R_y}\right)}\end{Bmatrix}d\mathcal{Z}$$

$$\{\mathfrak{V}_{53},\mathfrak{V}_{54},\mathfrak{V}_{55},\mathfrak{V}_{56},\mathfrak{V}_{57},\mathfrak{V}_{58}\} = \int_{-h/2}^{+h/2}\left(1+\frac{\mathcal{Z}}{R_x}\right)\frac{\mathbb{E}}{2(1+\vartheta)}\begin{Bmatrix}\frac{1}{R_x\left(1+\frac{\mathcal{Z}}{R_x}\right)},\frac{1}{R_y\left(1+\frac{\mathcal{Z}}{R_y}\right)},\mathcal{Z}\frac{1}{R_x\left(1+\frac{\mathcal{Z}}{R_x}\right)},\\ \mathcal{Z}\frac{1}{R_y\left(1+\frac{\mathcal{Z}}{R_y}\right)},\mathcal{Z}\frac{1}{2}\left(\frac{1}{R_x}-\frac{1}{R_y}\right)\frac{1}{R_x\left(1+\frac{\mathcal{Z}}{R_x}\right)},\\ \mathcal{Z}\frac{1}{2}\left(\frac{1}{R_x}-\frac{1}{R_y}\right)\frac{1}{R_y\left(1+\frac{\mathcal{Z}}{R_y}\right)}\end{Bmatrix}d\mathcal{Z}$$

$$\{\mathfrak{V}_{59},\mathfrak{V}_{60},\mathfrak{V}_{61},\mathfrak{V}_{62},\mathfrak{V}_{63},\mathfrak{V}_{64}\} = \int_{-h/2}^{+h/2}\left(1+\frac{\mathcal{Z}}{R_y}\right)\mathcal{Z}\frac{\mathbb{E}}{2(1+\vartheta)}$$

$$\left\{\begin{matrix}\frac{1}{R_x\left(1+\frac{Z}{R_x}\right)}, \frac{1}{R_y\left(1+\frac{Z}{R_y}\right)}, Z\frac{1}{R_x\left(1+\frac{Z}{R_x}\right)}, \\ Z\frac{1}{R_y\left(1+\frac{Z}{R_y}\right)}, Z\frac{1}{2}\left(\frac{1}{R_x}-\frac{1}{R_y}\right)\frac{1}{R_x\left(1+\frac{Z}{R_x}\right)}, \\ Z\frac{1}{2}\left(\frac{1}{R_x}-\frac{1}{R_y}\right)\frac{1}{R_y\left(1+\frac{Z}{R_y}\right)}\end{matrix}\right\}dZ$$

$$\{\mathfrak{V}_{65},\mathfrak{V}_{66},\mathfrak{V}_{67},\mathfrak{V}_{68},\mathfrak{V}_{69},\mathfrak{V}_{70}\}=\int_{-h/2}^{+h/2}\left(1+\frac{Z}{R_x}\right)Z\frac{\mathbb{E}}{2(1+\vartheta)}$$

$$\left\{\begin{matrix}\frac{1}{R_x\left(1+\frac{Z}{R_x}\right)}, \frac{1}{R_y\left(1+\frac{Z}{R_y}\right)}, Z\frac{1}{R_x\left(1+\frac{Z}{R_x}\right)}, \\ Z\frac{1}{R_y\left(1+\frac{Z}{R_y}\right)}, Z\frac{1}{2}\left(\frac{1}{R_x}-\frac{1}{R_y}\right)\frac{1}{R_x\left(1+\frac{Z}{R_x}\right)}, \\ Z\frac{1}{2}\left(\frac{1}{R_x}-\frac{1}{R_y}\right)\frac{1}{R_y\left(1+\frac{Z}{R_y}\right)}\end{matrix}\right\}dZ$$